Role of the Cytoplasmic Domain of the L1 Cell Adhesion Molecule in Brain Development

Yukiko Nakamura,[1] Suni Lee,[1,2] Candace L. Haddox,[1] Eli J. Weaver,[1,2] and Vance P. Lemmon[1,2]*
[1]The Miami Project to Cure Paralysis, University of Miami Miller School of Medicine, Miami, Florida 33136
[2]Department of Neuroscience, Case Western Reserve University, Cleveland, Ohio 44106

ABSTRACT

Mutations in the human L1CAM gene cause X-linked hydrocephalus and MASA (Mental retardation, Aphasia, Shuffling gait, Adducted thumbs) syndrome. In vitro studies have shown that the L1 cytoplasmic domain (L1CD) is involved in L1 trafficking, neurite branching, signaling, and interactions with the cytoskeleton. L1cam knockout ($L1^{KO}$) mice have hydrocephalus, a small cerebellum, hyperfasciculation of corticothalamic tracts, and abnormal peripheral nerves. To explore the function of the L1CD, we made three new mice lines in which different parts of the L1CD have been altered. In all mutant lines L1 protein is expressed and transported into the axon. Interestingly, these new L1CD mutant lines display normal brain morphology. However, the expression of L1 protein in the adult is dramatically reduced in the two L1CD mutant lines that lack the ankyrin-binding region and they show defects in motor function. Therefore, the L1CD is not responsible for the major defects observed in $L1^{KO}$ mice, yet it is required for continued L1 protein expression and motor function in the adult. J. Comp. Neurol. 518:1113–1132, 2010.

INDEXING TERMS: hydrocephalus; axon guidance; fasciculation; myelin; L1-CAM

The cell adhesion molecule L1 is a member of the immunoglobulin superfamily and is essential for development of the human and mouse nervous system (Dahme et al., 1997; Kamiguchi et al., 1998a; Kenwrick et al., 1996). In humans, mutations in the L1CAM gene cause X-linked hydrocephalus (OMIM #307000) and MASA syndrome (Mental retardation, Aphasia, Shuffling gait, Adducted thumbs; OMIM #303350). L1 has been implicated in different aspects of neural development, including neurite outgrowth (Lagenaur and Lemmon, 1987), axon fasciculation (Stallcup and Beasley, 1985), myelination (Barbin et al., 2004), and synapse formation (Godenschwege et al., 2006). These multiple functions of L1 depend on complex interactions with diverse molecules that associate with L1's extracellular and cytoplasmic domain (Hortsch et al., 2009; Maness and Schachner, 2007).

The extracellular domain participates in adhesion by homophilic interactions with L1 itself (Grumet and Edelman, 1988), or heterophilic interactions with CNTN2/axonin-1/TAG-1 (Kuhn et al., 1991), integrins (Ruppert et al., 1995), neuropilin-1 and SemaIIIa (Castellani et al., 2000), and other ligands (Haspel and Grumet, 2003).

The L1 cytoplasmic domain (L1CD) is highly conserved, being identical at the amino acid level in all mammals and shows strong conservation between invertebrates and vertebrates (Hortsch, 2000). Mutations in the L1CD cause MASA syndrome (Fransen et al., 1997). In neural tissue, the L1CD includes an alternatively spliced miniexon, RSLE, which is preceded by a tyrosine. The resulting YRSL sequence confers binding to a clathrin adaptor, AP-2 (Kamiguchi et al., 1998b) that is important in L1 trafficking (Dequidt et al., 2007; Kamiguchi et al., 1998b; Yap et al., 2008). L1 can be coupled to the actin cytoskeleton through interactions with either ankyrin 2 (Ank2) (Davis and Bennett, 1994; Yap et al., 2008) or ezrin-radixin-moesin (ERM) proteins (Dickson et al., 2002; Sakurai et al., 2008). Ank2 binding to L1 stabilizes its location on the cell surface (Gil et al., 2003; Hortsch et al., 2009; Scotland et al., 1998). ERM binding to L1 is important for L1-mediated axonal branching and guidance (Cheng et al., 2005a; Mintz et al., 2008).

Grant sponsor: National Institutes of Health; Grant number: HD39884; Grant sponsor: the Miami Project to Cure Paralysis; Grant sponsor: the RIKEN Brain Science Institute.

The first two authors contributed equally to this work.

*CORRESPONDENCE TO: Vance Lemmon, The Miami Project to Cure Paralysis, University of Miami Miller School of Medicine, Lois Pope LIFE Center (R48), 1095 NW 14th Terrace, Miami, FL 33136.
E-mail: VLemmon@med.miami.edu, vlemmon@gmail.com

Received 31 July 2009; Revised 18 September 2009; Accepted 29 October 2009
DOI 10.1002/cne.22267
Published online November 20, 2009 in Wiley InterScience (www.interscience.wiley.com).

TABLE 1.
Antibodies Used in This Study

Antibody Name	Antigen	Manufacturing details	Immunogen	Species	Working dilution
L1total	L1	V. Lemmon lab (Brittis et al., 1995)	Produced in the Lemmon lab to affinity purified Rat L1. Plasma membranes were prepared from P7 rat pups, solubilized in 1% TX-100 and run over a monoclonal anti-L1 column (mab 74-5H7). The rat L1 protein was eluted and used to immunize a rabbit.	Rabbit	1:5000
L1CD	L1 cytoplasmic domain	V. Lemmon lab (Schaefer et al., 2002)	Recombinant L1CAM cytoplasmic domain expressed in bacteria and purified on nickel column. the C-terminal 114 amino acids of human L1 used are: KRSKGGKYSVKDKEDTQVDSEARPMKDE TFGEYRSLESDNEEKAFGSSQPSLNGDI KPLGSDDSLADYGGSVDVQFNEDGSFIGQYSG KKEKEAAGGNDSSGATSPINPAVALE	Rabbit	1:5000
FIGQY	FIGQY	Gift from Dr. Matthew N. Rasband (Voas et al., 2007)	Peptide sequence CSFIGQYTVRK	Rabbit	1:200
L1ex	L1	Gift from Dr. Fritz Rathjen (Rathjen and Schachner, 1984)	Immunogen was mouse brain membranes	Rat	1:10000
clone 6C5	GAPDH	Ambion, Austin, TX, Cat#AM4300	Purified rabbit muscle GAPDH (whole molecule)	Mouse	1:10000
CantiTUJ1	beta-Tubulin3	Aves Labs, Tigard, Oregon, Cat#TUJ	Made against three synthetic peptides corresponding to different regions of the β-Tubulin 3 gene product, but are shared between the human (NP_AAL28094, NCBI) and rat (AAM28438, NCBI) protein sequences: TUJ#2: CZ SKV REE YPD RIM NTF S, TUJ#3: CZ KEV DEQ MLA IQS KNS SY, TUJ#4: CZ EAE SNM NDL VSE YQQ YQD	Chicken	1:1000
clone RT97	Neurofilament	Developmental Studies Hybridoma Bank, Iowa City, IA, Cat#RT97	Semipurified neurofilament from Wistar rat brains.	Mouse	1:1000

Because numerous studies implicate the cytoplasmic domain of L1 in the protein's function and human mutations in the L1CD cause central nervous system (CNS) deficits, we were motivated to generate three new mutant mice lines. One line has a point mutation (Y1176>A) previously shown in vitro to influence L1 trafficking and interaction with ERMs. The other two lines have truncations that remove approximately one-half or nearly the entire L1CD ($L1^{1180}$ and $L1^{1152}$, respectively). We examined the brains of the L1CD mutant mice, focusing on regions that show abnormalities in $L1^{KO}$ mice. Surprisingly, we observed none of the gross morphological or histological abnormalities in the CNS or peripheral nervous system (PNS) that are present in $L1^{KO}$ mice. All the L1CD mutant mice express L1 protein in the usual pattern in young animals, but expression of L1 protein in adults is very low in the two L1CD mutant lines that lack the Ank2 binding region. In addition, these two L1CD mutant lines showed a defect in motor function. These data show that the L1CD is not essential for several interesting defects present in $L1^{KO}$ mice, but is critical for sustained L1 protein expression, which in turn may be necessary for motor coordination.

Abbreviations

BDA	biotinylated dextran amine
CNS	central nervous system
CST	corticospinal tract
ERM	ezrin-radixin-moesin
L1-CAM	L1 cell adhesion molecule
L1CD	L1 cytoplasmic domain
L1ED	L1 extracellular domain
$L1^{KO}$	L1cam knockout
MASA syndrome	Mental retardation, Aphasia, Shuffling gait, Adducted thumbs
Ng-CAM	neural glial cell adhesion molecule
PNS	peripheral nervous system
WT	wild type

MATERIALS AND METHODS

Antibody characterization

Primary antibodies (Table 1) include:

Rabbit anti-L1total (Brittis et al., 1995), produced in the Lemmon lab.

Rabbit anti-L1CD (Schaefer et al., 2002), produced in the Lemmon lab to recombinant L1 cytoplasmic domain.

Rabbit anti-FIGQY (gift from Dr. Matthew N. Rasband; Ogawa et al., 2006), produced to a small peptide corresponding to a highly conserved cytoplasmic sequence found in all L1-CAMs.

Rat anti-L1ex (gift from Dr. Fritz Rathjen; Lindner et al., 1983; Rathjen and Schachner, 1984), the original monoclonal antibody to mouse L1 made by Fritz Rathjen.

All of the antibodies to L1 have been tested and do not bind to Western blots of $L1^{KO}$ brain membranes (for example, see Fig. 9). When used to immunoprecipitate mouse brain, they give only proteins with the expected bands at 220, 180, and 80 kDa. The anti-FIGQY antibody recognizes the L1 family members and when immunoprecipitation was also performed with the L1ex antibody, only the expected bands at 220 and 80 kDa were observed.

Other antibodies were as follows:

Mouse anti-GAPDH (cat. no. AM4300, 1:10,000; Ambion, Austin, TX) antibody was used as a loading control for Western blots and only detected a single band at the expected molecular weight at about 39 kDa.

Chicken anti-β-tubulin 3 (cat. no. TUJ, 1:1,000; Aves Labs, Tigard, Oregon). When used to visualize neurites in culture, it gave the expected staining pattern and did not stain glia or fibroblasts.

Mouse anti-neurofilament (RT97, 1:1,000) obtained from the Developmental Studies Hybridoma Bank (Iowa City, IA). When used to stain axons in brain sections to examine fasciculation, it gave the expected staining pattern, consistent with earlier reports (Johnstone et al., 1997; Shin et al., 2003).

Animals

All animal experiments described in this manuscript have been approved by the Case Western Reserve University and the University of Miami IACUCs. $L1^{Y1176A}$, $L1^{1180}$, and $L1^{1152}$ mice were generated by using a Cre/lox approach (Fig. 1A). The L1cam gene has 29 exons, 28 of which are coding and one of which contains a 5′ untranslated sequence (Meech et al., 1999). The 9.7 kb of *Xba*I DNA fragment including exons 12–29 was obtained from a 129/SvJ genomic BAC clone containing the entire L1cam gene (Caltech 129/SvJ mouse genomic library clone Citb/CJ7/567G9, purchased from Open Biosystems, Huntsville, AL). A fragment from *Pml*I located in exon 14 and a *Psh*A I located at 2.1kb downstream from the stop codon were chosen as the ends of the 5′ and 3′ arms, respectively. A mutated fragment was substituted for corresponding wild-type sequences. A neomycin resistance cassette, with an MC1 promoter and polyadenylation signal and flanked loxP sites, was inserted into the *Bgl*I site located between exons 26 and 27 for positive selection. To provide for negative selection, the L1cam 5′ arm neomycin resistance cassette/L1cam 3′ arm fragment (9.4 kb) was replaced with a neomycin cassette of pPNT (Tybulewicz et al., 1991) containing the HSV-Thymidine kinase gene with the phosphoglycerate kinase-1 promoter.

Following digestion with *Not*I, the linearized construct was electroporated into embryonic stem cells (ES PC3 cells [Protamine-Cre recombinase transgene including embryonic stem cells]' O'Gorman et al., 1997). ES cells were cultured in G418-containing media, and surviving cells were screened by Southern hybridization. The wild-type (WT) gene has a 9.7-kb *Xba*I-*Xba*I fragment. The mutant gene generates an *Xba*I site in the lox P cassette, so after *Xba*I digestion it gives a shorter fragment. Two probes were prepared for confirmation of 5′ and 3′ recombination. Probe L, detecting a 5′ homologous recombination, is 0.6 kb upstream of the *Pml*I site, and probe R, detecting 3′ homologous recombination, is 0.9 kb downstream of the *Psh*AI site. The probes detect 5.6-and 5.3-kb fragments, respectively.

Prior to initiating analysis of the three lines, the mice were backcrossed onto the 129S2/Sv (129S2/SvPascrlf) and the C57BL/6 background by using MAX-BAX (Marker-Assisted Accelerated Backcrossing) speed congenics (Charles River, Wilmington, MA) until the lines were congenic.

Mutagenesis

First, 0.3 kb of a *Bam*HI/*Sac*I fragment containing exons 27 and 28 was subcloned into pBluescript SK+ (Stratagene, La Jolla, CA) for the mutagenesis template. Oligonucleotides were designed for the mutagenesis containing a mutation that generates a stop codon just before RSLE, 5′-GACCTTCGGCGAGTACTAGTGAGCAGGGACAAA AG-3′ and 5′-CTTTTGTCC CTGCTCACTAGTACTCGCCGAAGGTC-3′, 1176 Tyr residue changed into Ala, 5′-GAGACCTTCGGCGAGGCCAGGTGAGCAGGGAC-3′ and 5′-GTCCCTGCTCACCTGGCCTCGCCGAAGGTCTC-3′, and a stop codon just after RSLE, 5′-GACTTCAGGTCCCTGGAGTAGGTAAGATGTGACAGTAGG-3′ and 5′-CCTACTGTCACATCTTACCTACTCCAGGGACCTGAAGTC-3′. The QuickChange II Site Directed Mutagenesis Kit (Stratagene) was used following the manufacturer's instructions. Each mutated fragment was substituted with original (wild-type) *Bam*HI and *Sac*I sites of corresponding DNA sequences.

Preparation of membrane proteins

Mouse brain homogenates were prepared by homogenizing brains in a buffer containing 50 mM Tris (pH 7.2), 0.32 M sucrose, and protease inhibitor (Roche Diagnostics, Indianapolis, IN). The solution was layered over a sucrose gradient consisting of two discontinuous layers of 0.8 M and 1.2 M sucrose dissolved in 50 mM Tris, pH 7.2, and centrifuged at 40,500*g* for 1.5 hours in a Beckman (Fullerton, CA) SW 28. The membrane fraction at the 0.8–1.2 M sucrose interface was collected and diluted with 1 vol of 50 mM Tris, pH 7.2, and then centrifuged at 230,000*g* for 20 minutes in a Beckman Ti 70.1. For some experiments the membrane pellets were resuspended in 0.1 M PBS. For other experiments, the pellets were resuspended in 1% Triton X-100, 50 mM Tris, pH 8.0, sonicated,

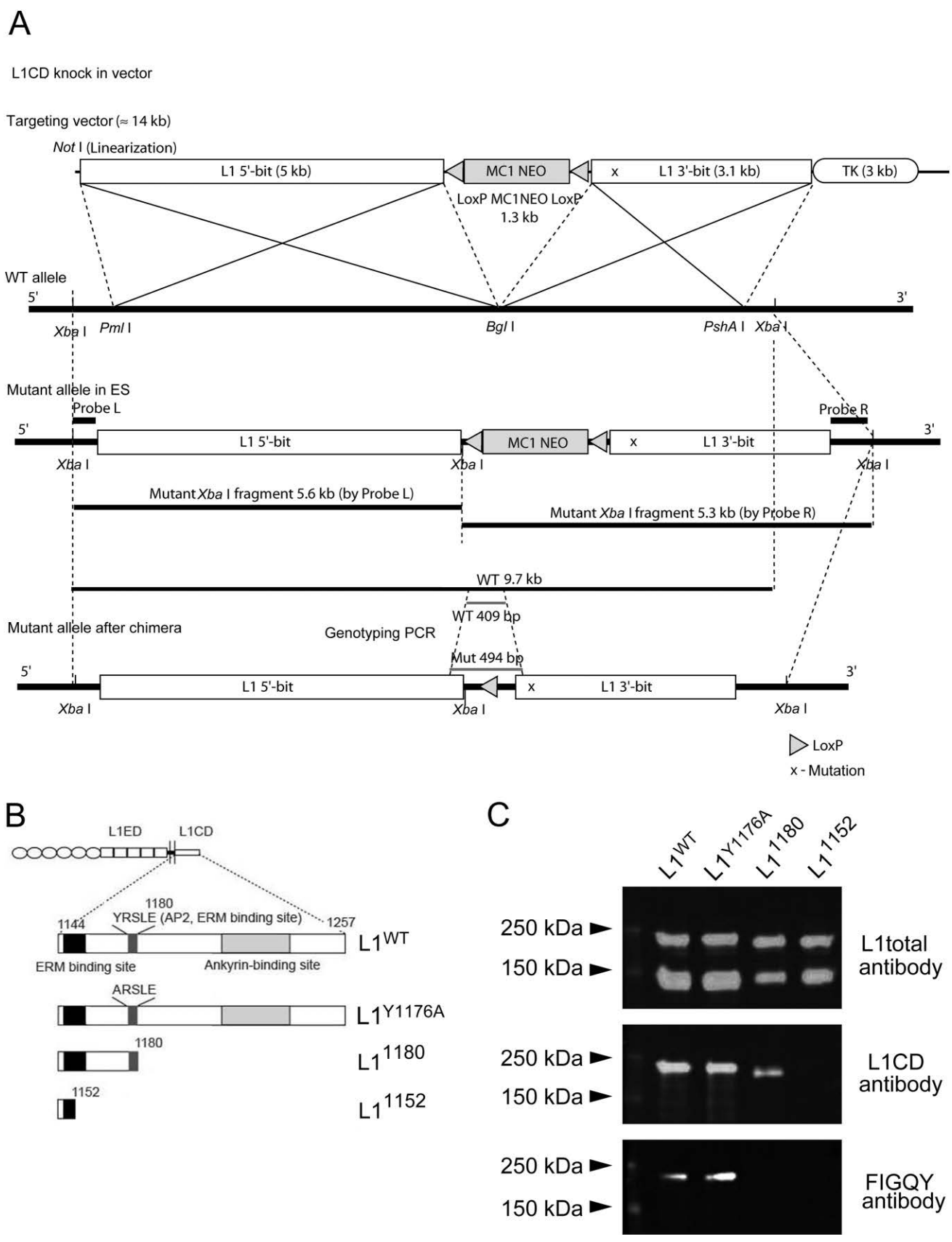
A
L1CD knock in vector
Targeting vector (≈ 14 kb)
Not I (Linearization)
L1 5'-bit (5 kb)
MC1 NEO
x
L1 3'-bit (3.1 kb)
TK (3 kb)
LoxP MC1NEO LoxP
1.3 kb
WT allele
5'
3'
Xba I
PmlI
BglI
PshA I
Xba I
Mutant allele in ES
Probe L
Probe R
5'
L1 5'-bit
MC1 NEO
x
L1 3'-bit
3'
Xba I
Xba I
Xba I
Mutant Xba I fragment 5.6 kb (by Probe L)
Mutant Xba I fragment 5.3 kb (by Probe R)
WT 9.7 kb
WT 409 bp
Mutant allele after chimera
Genotyping PCR
Mut 494 bp
5'
L1 5'-bit
x
L1 3'-bit
3'
Xba I
Xba I
Xba I
LoxP
x - Mutation
B
L1ED
L1CD
1180
YRSLE (AP2, ERM binding site)
1144
1257
L1WT
ERM binding site
Ankyrin-binding site
ARSLE
L1Y1176A
1180
L1 1180
1152
L1 1152
C
L1WT
L1Y1176A
L1 1180
L1 1152
250 kDa
150 kDa
L1total antibody
250 kDa
150 kDa
L1CD antibody
250 kDa
150 kDa
FIGQY antibody

Figure 1

and centrifuged at 230,000*g* for 30 minutes. The supernatant (membrane extract) was reserved for subsequent use.

Immunoprecipitation

For some Western blot experiments, L1 immunoprecipitation was performed. Protein A-sepharose beads (Pierce, Rockford, IL) were coated with L1ex antibody, which recognizes the extracellular region of L1 (Rathjen and Schachner, 1984). The L1ex-coated beads were incubated with membrane extract at 4°C overnight, spun down, and washed with 1% Triton X-100 in 50 mM Tris, pH 8.0. Protein was eluted by adding 2X sodium dodecyl sulfate-polyacrylamide gel electrophoresis (SDS-PAGE) sample buffer (100 mM Tris-HCl, pH 6.8, 4% SDS, 0.2% bromophenol blue, 5% glycerol, and 12% 2-mercaptoethanol) and heating at 100°C for 5 minutes.

Western blotting

The membrane extracts were subjected to SDS-PAGE and Western blotting either directly or after immunoprecipitation. Samples were separated by electrophoresis in 8.5% polyacrylamide gels and transferred to PVDF membrane (Millipore, Bedford, MA). Membranes were blocked at room temperature for 30 minutes with Odyssey blocking buffer (LI-COR, Lincoln, NE). Blots were then incubated with primary antibody in Odyssey blocking buffer at 4°C overnight. Primary antibodies used include: anti-L1total (1:5,000; Brittis et al., 1995), anti L1CD (1:5,000; Schaefer et al., 2002), anti-FIGQY (1:200; Voas et al., 2007), anti L1ex (1:10,000; Lindner et al., 1983), and anti-GAPDH (1:10,000; Ambion). For detection, the blots were incubated with secondary antibody for either anti-rabbit (1:5,000), or anti-rat (1:500), or anti-mouse (1:5,000) IRdye800 or IRdye700 (L1-COR) at room temperature for 1 hour, and then scanned by using an Odyssey infrared imaging machine (L1-COR).

Figure 1. Production of L1CD mutant mice. **A:** Schematic model of the strategy used to mutate the L1cam gene. The bold line indicates the wild-type allele, and the corresponding fragment of the targeting vector is depicted in the white box. (X) in "3′-bit" fragment indicates mutated region. A loxP-neomycin cassette was inserted with reverse orientation into the *BglI* site located between exon 26 and exon 27 for positive selection. Probes L and R were prepared for confirmation of 5′ and 3′ recombination. *Xba* I digestion gives a 9.7-kb wild-type fragment, whereas the mutant allele gives a 5.6-kb 5′ fragment and a 5.9-kb 3' fragment. Primers for genotyping PCR were designed to amplify a 409-bp wild-type fragment and a 494-bp mutant fragment. Cre-recombinase regulated by the protamine promoter is carried by ES cells and removes the loxP-Neo cassette once it is integrated into the chimera sperm (germ line). **B:** Schematic representation of L1cam in the L1CD mutant mice. The amino acid numbers correspond to their position in the L1CD of $L1^{WT}$ (amino acids 1144–1257). The juxtamembrane region, the ERM binding site, the ankyrin binding site, and the AP-2 binding site are highlighted. The numbers of the key residues are indicated on top of the corresponding residue. The $L1^{Y1176A}$ mice have a single amino acid substitution. The $L1^{1152}$ mice have a truncation after the S1152 residue. The $L1^{1180}$ mice have truncation after the E1180 residue. **C:** Western blot analysis from whole brain after immunoprecipitation using L1ex antibody. Three different antibodies were used for characterization of $L1^{WT}$, $L1^{Y1176A}$, $L1^{1180}$, and $L1^{1152}$ mice. L1 total polyclonal antibody recognizes L1 extracellular and intracellular regions, L1CD polyclonal antibody recognizes the cytoplasmic region of L1, and FIGQY monoclonal antibody recognizes the FIGQY region in the ankyrin binding site.

Preparation of substrate

For these experiments we used Human L1-Fc or laminin for the substrate. For L1-Fc substrate, anti-human-Fc (Rockland, Gilbertsville, PA; 8 μg/well) was incubated in 96-well plates (Packard View Plates, Packard BioScience, Meriden, CT) overnight at room temperature. Following several washes with PBS, L1-Fc (4 μg/well) was incubated overnight at room temperature. For laminin substrate, poly-D-lysine (100 μg/ml) was incubated in 96-well plates (Packard View Plates) or on cover glass overnight at room temperature. Following several washes with Hank's balanced salt solution (HBSS), laminin (10 μg/ml) was incubated overnight at room temperature. Plates or coverslips were washed with PBS before the neurons were plated.

Primary hippocampal cultures

Postnatal day 2–3 mouse hippocampi were removed in Hibernate E (Brain Bits, Springfield, IL) and incubated with 20 U/ml papain (Worthington, Freehold, NJ) and 0.1 mg/ml DNase (Sigma-Aldrich, St. Louis, MO) for 30 minutes at 37°C, followed by washing with Hibernate E and 1X B27 (Invitrogen, Carlsbad, CA) and incubation with 0.25% trypsin (Invitrogen). After washing with Hibernate E and B27, cells were incubated for 3 days with Enriched Neurobasal (ENB) media (1X penicillin-streptomycin liquid [Invitrogen], 1X insulin [Sigma-Aldrich], 1 mM sodium pyruvate [Invitrogen], 1X T3 [Sigma-Aldrich], 1X L-glutamine [Invitrogen], 1X NAC [Sigma-Aldrich], 1X B27 [Invitrogen], 4 mg transferrin [Sigma-Aldrich], 4 mg bovin serum albumin [BSA; Sigma-Aldrich], 2.5 μg progesterone [Sigma-Aldrich], 0.64 mg putrescine [Sigma-Aldrich], 1.6 μg sodium selenite [Sigma-Aldrich]).

Immunostaining for hippocampal primary cultures

The cultures were fixed with 4% paraformaldehyde (PFA; Sigma-Aldrich), 4% sucrose (Sigma-Aldrich), in phosphate-buffered saline (PBS) for 15 minutes. Neurons were blocked with 0.03% Triton-X and 0.2% gelatin at room temperature for 1 hour, followed by incubation with primary antibody at 4°C overnight and secondary antibody at room temperature for 1 hour. Primary antibodies were used for

immunostaining as follows: L1total (1:100; Brittis et al., 1995), anti-βtubulin 3 (1:1,000; Aves Labs), and anti-neurofilament (RT97, 1:1,000).

Semiquantitative measurements of L1 expression on hippocampal neurons

To measure the intensity of L1 and tubulin, hippocampal neurons from all three mutant mice and $L1^{WT}$ mice were prepared, cultured, and stained on the same day by using the same conditions and antibodies. Images were acquired by using a Zeiss LSM 410 confocal microscope. The intensity of L1 and tubulin was measured by MetaMorph software (Molecular Devices, Sunnyvale, CA) with no adjustments to the acquired images. To produce the magenta/green images for Figure 2, the red/green images obtained from the LDM 410 were imported into Photoshop (10.0 for the Mac; Adobe Systems, San Jose, CA), and the red channel was adjusted so the brightest pixels were about 250. The red channel was then imported into ImageJ (1.42 for the Mac; National Institutes of Health, Bethesda, MD), and the red channel was copied into the blue channel to produce magenta. Finally, the red and blue channels were merged in ImageJ with the green channel to give the magenta/green/white images that show co-localization of L1 and tubulin.

Morphometery of hippocampal neurons

Images of neurons in 96 wells were taken and analyzed by using a Cellomics VTI Arrayscan High Content Screening Microscope (Thermo Fisher Scientific, Pittsburgh, PA). These data were analyzed by Spotfire software (Tibco, Palo Alto, CA). Parameters of special interest were the longest neurite length, neurite total length, number of branches of the neurites, and number of neurites emerging from the soma.

Immunohistochemistry

Fixation and staining were performed as described previously (Nakamura et al., 2006). Briefly, young mice (7 days of age) and adult mice (7 weeks of age) were anesthetized by an i.p. injection of ketamine and xylazine, and perfused transcardially with 4% PFA in PBS. Brains were removed and postfixed at 4°C overnight in the same fixative, followed by immersion in 30% sucrose. Frozen 30-μm-thick coronal sections were used for immunohistochemistry. The sections were blocked in 5% BSA in PBS, and incubated with primary antibodies at 4°C overnight. Sections were rinsed in PBS and incubated in biotinylated secondary antibodies at 4°C over night (1:500; Vector, Burlingame, CA). Bound antibodies were detected by staining for 2 hours with the ABC Vectastain kit (Vector) and then for 5 minutes with 0.05% 3,3′-diaminobenzidine tetrahydroxychloride (DAB) in 50 mM Tris-HCl, pH 7.5, containing 0.01% H_2O_2. Primary antibodies were used for immunostaining as follows: L1ex (1:2,000; Lindner et al., 1983) and anti-neurofilament (RT97, 1:1,000).

Real-time quantitative PCR analysis

cDNA was produced from 7-week-old mouse brains by a reverse transcription polymerase chain reaction (PCR) kit (Invitrogen) according to the manufacturer's instructions. Quantitative reverse transcriptase-PCR (qRT-PCR) was performed by using the QuantiFast SYBR Green RT-PCR Kit (Qiagen, Valencia, CA). Expression data were normalized to β-actin. The primers were as follows: L1cam left: 5′-accctgaggcattacacctg-3′, L1cam right: 5′-agttctgggtccgaaaggtt-3′.

Morphological and histological analysis

For detection of hydrocephalus, brains were cut coronally at −0.9 mm from bregma. To examine the cerebellum and corpus callosum, brains were cut sagittally at the midline. The brains were observed with a stereo microscope (Wild Heerbrugg-M650 microscope, Leica Geosystems, Norcross, GA), imaged with a Spot 2.3.0 camera and SPOT software (Diagnostic Instruments, Sterling Heights, MI). To measure the area of the cerebellum, digital images from the midline were traced with ImageJ software. To measure the pyramidal tract, coronal serial slices were obtained at 30-μm-thickness by using a Vibratome, after PFA perfusion. Wet slices in 0.1 M PBS, pH 7.4, were put on glass slides, allowing the pyramidal tract to be detected microscopically (using an Olympus BX51 light microscope, and image capture with a Microfire camera [Optronics, Goleta, CA]). Images of the pyramidal tract just rostral to the decussation were collected, and the cross-sectional area was traced with ImageJ software.

Pyramidal tract tracing

Mice were anesthetized with a ketamine/xylazine cocktail by i.p. injection. The skull was opened, and 10% biotin-conjugated dextran amine (BDA; MW 10,000; Molecular Probes, Eugene, OR) was injected into three sites (1 μl/site) into the motor cortex by using a Hamilton (Reno, NV) syringe. After surgery, the mice were kept on a heating pad until completely recovered from anesthesia. Mice were transcardially perfused 6 days after injection of BDA, and then 20-μm coronal sections were taken. BDA was detected by using streptoavidin Alexa Fluor 594 conjugate (1:200; Invitrogen).

Electron microscopy

Sciatic nerves of adult mice were removed and fixed at 4°°C in 2% PFA, 2% glutaraldehyde in 0.1 M PBS, pH 7.4. Then sciatic nerves were put in 2% OsO_4 for 1 hour at room temperature before being embedded in Embed plastic

(Electron Microscopy Sciences, Fort Washington, PA). Thin sections were stained with uranyl acetate and lead citrate and examined by using a Philips CM-10 electron microscope (FEI Company, Hillsboro, OR).

g-ratio

For measuring the g-ratio, 1-μm semithin sections of sciatic nerve were prepared and stained with toluidine blue/methylene blue/sodium borate. Threshold images were obtained with ImageMagick software (ImageMagick Studio, Landenberg, PA). For measurement of the g-ratio (ratio of myelin thickness to axon size), the threshold images were measured with ImageJ software.

Spatial learning and memory in the radial-arm water maze

The radial six-arm water maze is a hybrid of the Morris water maze and a radial arm maze, which combines the simple motivation provided by water immersion along with scoring errors obtained with a radial arm maze (Alamed et al., 2006). Each mouse was placed on the platform for 20 seconds, followed by a 1-minute swimming period starting from each arm and ending when the mouse found the platform. This session was repeated three times during 3 successive days of training, followed by one test trial on each of the next 2 days.

Motor function

Mice were placed on a rotating rod (IITC 755 Rotarod, IITC Life Sciences, Woodland Hills, CA) facing the opposite direction to the motion of the rod, which was set to accelerate from 0 to 30 rpm over 3 minutes. Automatic timers scored the latency for the mice to fall off the rod into the chamber below. Mice were trained for 2 weeks and then tested for 1 week, with one trial per day.

Statistics

In all cases analysis of variance was performed with the level of significance set at 0.05.

RESULTS

Production of three kinds of L1CD mutant mice: $L1^{Y1176A}$, $L1^{1180}$, and $L1^{1152}$

We generated three L1CD mutant mice (Fig. 1). In our experimental design we wanted to make mutations with a minimum impact on L1cam gene organization to reduce the possibility of altered gene expression and/or other unanticipated complications. Initially we chose to focus on making constructs that would distinguish between the roles of Ank2 and the critical region at the RSLE mini-exon that is involved in clathrin-mediated endocytosis and ERM binding. The $L1^{Y1176A}$ mice had one amino acid substitution from tyrosine to alanine, therefore lacking the AP-2 binding site and a site involved in ERM interactions with L1, but preserving the rest of the L1CD. The other two L1CD mutant mice had truncation mutations. $L1^{1180}$ mice have a stop codon after the E1180 codon, thereby preserving binding to AP-2 and ERM proteins but not binding to Ank2 or RanBPM.

Our original plan was to produce a mutant line with a truncation at Y1176, i.e., before the mini-exon that codes for RSLE. This required altering the sequence at the end of exon 28 by converting Y1176 to a stop codon. Sequencing of genomic DNA from the three new lines confirmed that they all had the expected mutations that were introduced into the ES cells (data not shown). It is well established that the genetic background influences the phenotype of L1cam mutant mice. Consequently, we backcrossed the mice onto 129S2/Sv (129S2/SvPascrlf) and C57BL/6J by using speed congenics, and only performed experiments on mice that were at least 98% congenic, based on analysis of 110 microsatelitte markers.

Next we checked the sequence of the L1 mRNA from the three new mutant mice lines. The sequence of the mRNA for $L1^{Y1176A}$ and $L1^{1180}$ was the expected sequence based on our design and the sequence of the genomic DNA. However, the sequence of the putative $L1^{1176}$ was not. Instead, the L1 sequence ended at what corresponds to exon 26, followed by 78 apparently random nucleotides. We conclude that the mutation introduced at the end of exon 26 disrupted splicing, leading to skipping of exon 27. Although the resulting mice were not what we had originally planned, indeed we believe they are even more informative because the introduced mutation resulted in the elimination of 105/114 of the highly conserved amino acids in the L1CD. Henceforth we will refer to this mutant as $L1^{1152}$.

Western blotting was performed on the new lines to confirm that L1 protein was expressed. For the initial characterization, several antibodies against different regions of L1 were used for Western blotting. To reduce the background and increase the band density for Western blotting, we immunoprecipitated L1 from mouse brain extracts. This experiment does not provide information about the expression level of L1 protein in different L1cam mice lines, but does provide information about whether these mutant mice express L1 protein of the expected size. With a polyclonal antibody to L1, $L1^{WT}$, all three L1CD mutant mice showed two clear L1 bands, ~220 kDa (full-length L1) and ~140 kDa (cleaved form of L1) (Fig. 1C), whereas $L1^{KO}$ mice did not show any bands (data not shown, but see Itoh et al, 2004). The two lines with truncated L1 ($L1^{1180}$ and $L1^{1152}$) showed bands at lower molecular weights $L1^{WT}$, as expected. With a polyclonal antibody that recognizes the L1CD, $L1^{1152}$ did not show any band, demonstrating that $L1^{1152}$ mice lack the majority of the L1CD.

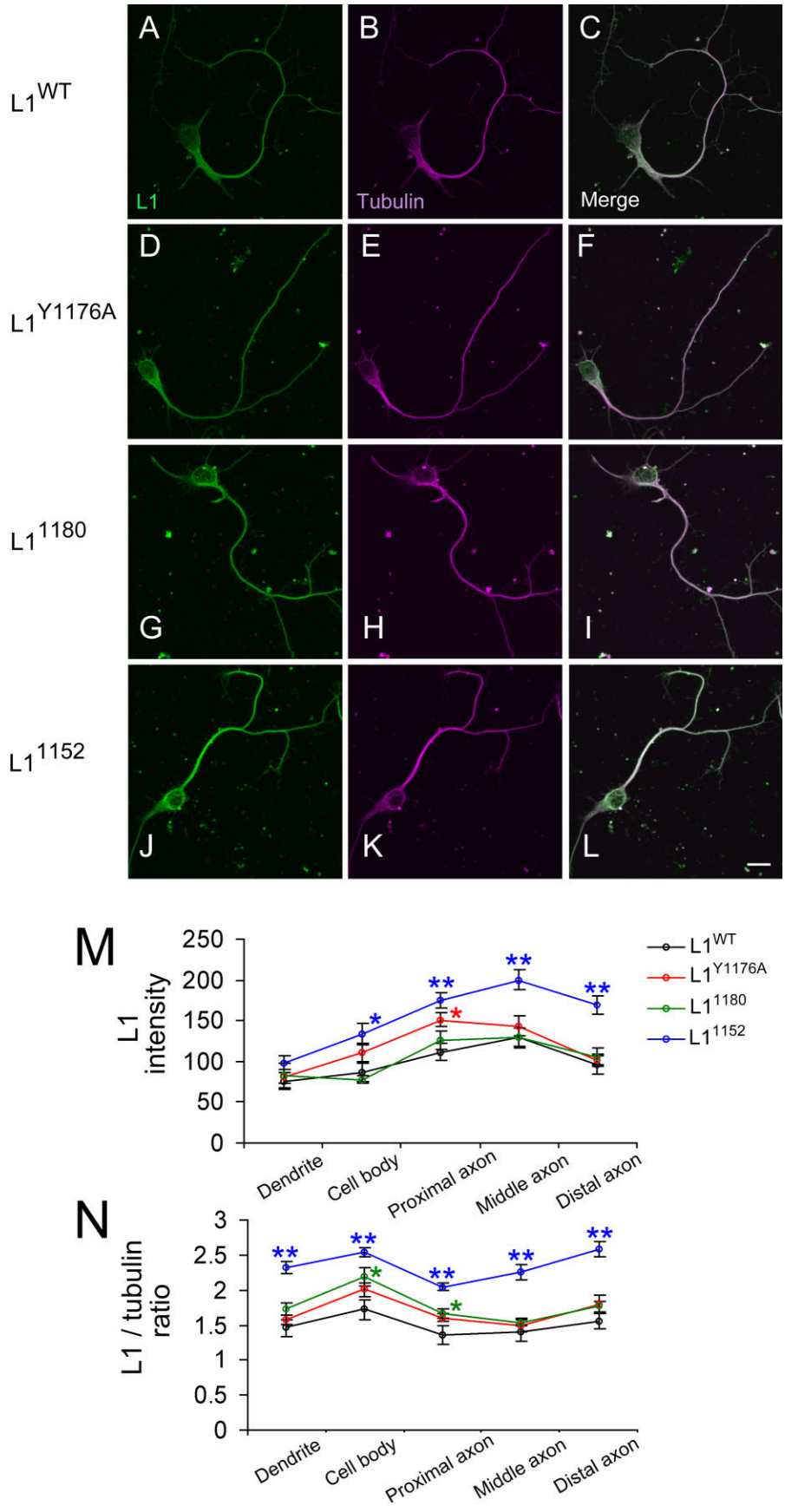
L1WT
L1Y1176A
L1 1180
L1 1152
A
B
C
D
E
F
G
H
I
J
K
L
L1
Tubulin
Merge
M
L1 intensity
250
200
150
100
50
0
Dendrite
Cell body
Proximal axon
Middle axon
Distal axon
L1WT
L1Y1176A
L1 1180
L1 1152
N
L1 / tubulin ratio
3
2.5
2
1.5
1
0.5
0

Figure 2

With the FIGQY monoclonal antibody that recognizes the FIGQY sequence in the Ank2 binding site, only $L1^{WT}$ and $L1^{Y1176A}$ mutant mice showed L1 bands. Therefore, the data for the sequence of L1 mRNA and Western blotting show that 1) L1 protein is expressed in the brains of the three new lines; 2) $L1^{Y1176A}$ mutant protein has a similar molecular weight to $L1^{WT}$; 3) $L1^{1180}$ has a truncation missing the Ank2 binding region; and 4) $L1^{1152}$ has a larger truncation.

L1 protein in hippocampal neurons is transported into axons in L1CD mice

It has been shown that the transportation of L1 from the cell body to the neurites is inhibited by mutating the extracellular domain of L1 (C264Y), leading to L1 being concentrated in the cell body (Runker et al., 2003). It has also been shown in dorsal root ganglion (DRG) neurons that disruption of the tyrosine-based sorting motif prevented transport of L1 into neurites (Kamiguchi and Lemmon, 1998), whereas similar mutations in Ng-CAM had less of an effect in hippocampal neurons (Sampo et al., 2003; Wisco et al., 2003; Yap et al., 2008). To determine whether the L1CD is necessary for transport of L1 from the cell body into axons, we examined cultured hippocampal neurons and assessed the distribution of L1 in axons. After 3 days in culture, axons and dendrites were distinguishable based on morphological and immunohistochemical criteria on laminin substrates (Dotti et al., 1987). An axon was observed in cultured hippocampal neurons from all three L1cam mutant mice, and L1 was observed all the way to the growth cone of the longest neurites, similar to $L1^{WT}$ mice (Fig. 2A). Additionally, the intensity of L1 immunoreactivity in L1CD mice was comparable to that of $L1^{WT}$ mice (Fig. 2D,G,J). Interestingly, the $L1^{1152}$ mutant actually has higher expression in the axon than $L1^{WT}$ under these conditions (Fig. 2M,N), in contrast to the situation in the adult brain (see below). These results showed that L1CD mutant mice can express L1 protein similar to $L1^{WT}$ mice and that the L1CD is not essential for the transportation of L1 from the cell body to the axon.

Figure 2. Normal L1 protein expression in hippocampal neurons from L1CD mutant mice. **A–L:** Hippocampal culture on laminin substrate at 3 days in vitro. These neurons are stained by anti-L1 total antibody (A,D,G,J) and anti-β-tubulin 3 antibody (B,E,H,K). **A–C:** WT. **D–F:** $L1^{Y1176A}$. **G–I:** $L1^{1180}$. **J–L:** $L1^{1152}$. The merged images are shown in C,F,I,L. **M:** Intensity of L1 in several regions (dendrite, cell body, proximal axon, middle axon, and distal axon). Fifteen neurons each from the L1CD lines and $L1^{WT}$ were analyzed by using confocal images. **N:** Relative amount of L1 intensity, which is normalized to the tubulin intensity. All L1CD mutant mice could produce and transport L1 protein into axons. *, $P < 0.05$; **, $P < 0.001$. Scale bar = 10 μm in L (applies to A–L).

The L1CD is important for L1-mediated neurite extension and branching

The L1CD has been implicated in neurite extension and branching, which could be important for pathfinding of axons during brain formation (Kamiguchi and Lemmon, 2000b; Wiencken-Barger et al., 2004; Buhusi et al., 2008). To examine the role of L1CD in neurite outgrowth, hippocampal neuronal morphology was examined. These cultures were grown on laminin for 3 days (Fig. 3A–D). We focused on four categories (longest neurite length, neurite total length, number of branches from neuritis, and number of neurites extending from the soma) to characterize neuronal morphology. The methods used to trace and analyze neuronal morphology automatically using High Content Analysis methodologies have the advantages of providing large numbers of cells and no investigator bias. However, they also have some limitations in that staining with axonal markers, such as anti-Tau, are not possible because the software cannot connect the Tau staining to the somas in a reliable way. As a result, we cannot make strong statements about branching of axons versus dendrites. Nonetheless, if the morphological criteria of Dotti and Banker regarding E18 rat hippocampal neurons (Dotti et al., 1987) can be applied to our slightly older (P3) mouse hippocampal neurons, it is likely that the large differences in branching are in axons and not dendrites.

The longest neurite length and number of neurites extending from the soma were not perturbed in L1CD mutant mice, but the number of branches was reduced (~20%) in $L1^{1152}$ mice. This particular result was not anticipated, but Grumet and colleagues (1993) have previously reported that antibodies to Ng-CAM, the chick homologue of L1, can perturb growth on laminin, and it is well established that L1 interacts with integrins (Montgomery et al., 1996), so this may account for this observation. Neurite outgrowth was significantly greater on L1-Fc substrates compared with laminin (Fig. 3). The length of the longest neurite was increased in neurons from all three L1CD mutant mice on L1-Fc substrate, which shows that the cytoplasmic region of L1 is not essential for neurite extension on L1 substrates. Interestingly, the number of branches in $L1^{1152}$ neurons was not enhanced on L1-Fc substrate compared with laminin. However, $L1^{Y1176A}$ and $L1^{1180}$ neurons showed an increase in the number of branches on an L1 substrate compared with laminin, similar to $L1^{WT}$. These data indicate that the juxtamembrane ERM binding site (Cheng et al., 2005a) has an important role in L1-dependent neurite branching but the ERM binding site involving the YRSL region does not (Dickson et al., 2002). The data from the $L1^{1180}$ and $L1^{1152}$ hippocampal neurons are similar to data reported by using overexpression approaches in cerebellar granule cells (Cheng et al., 2005a)

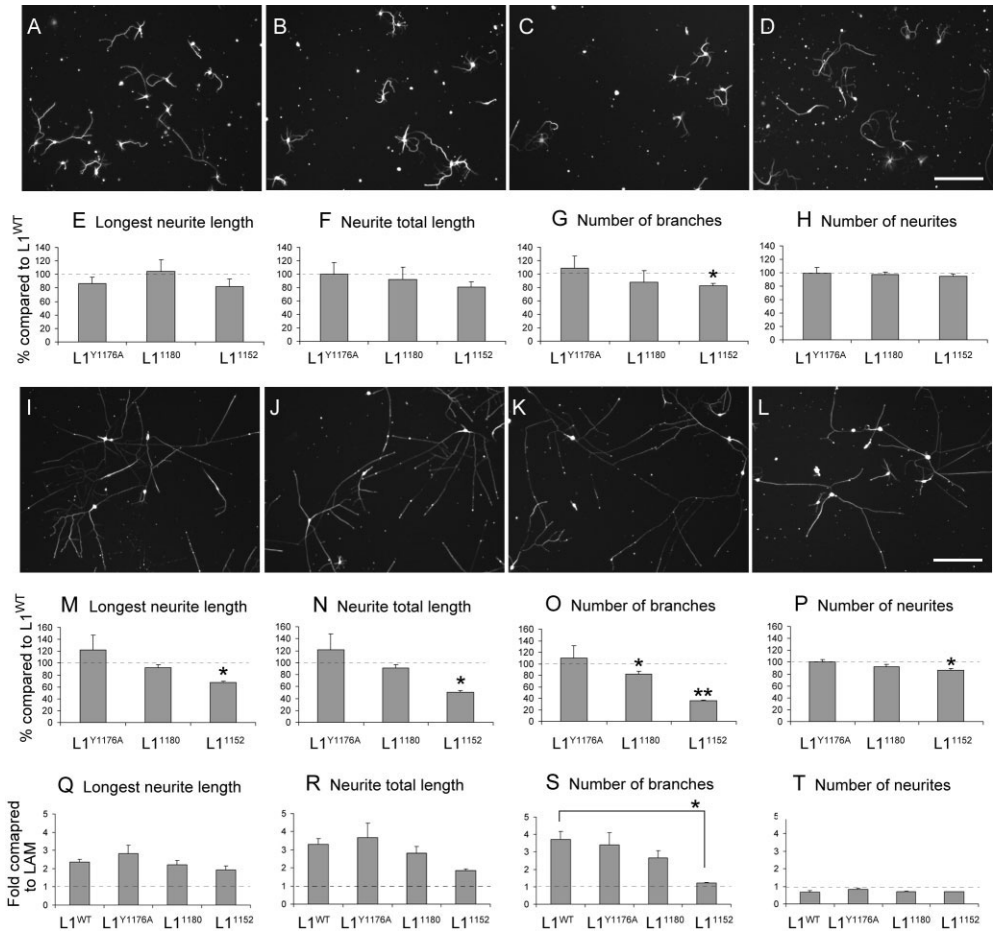

Figure 3. Neurite branching on L1 substrates is impaired in $L1^{1152}$ mutant mice. A,I: WT. B,J: $L1^{Y1176A}$. C,K: $L1^{1180}$. D,L: $L1^{1152}$. **A–D:** Hippocampal neuronal culture grown on laminin substrate at 3 days in vitro (DIV). Neurons are stained with anti-β-tubulin 3. **E–H:** The total neurite length, longest neurite length, number of neurite branches, and number of neurites extending from soma are quantified. The mean values of neurons of L1CD mutant mice are normalized to mean values of neurons of $L1^{WT}$ mice. *, $P < 0.05$. **I–L:** Hippocampal neuronal culture grown on L1-Fc substrate at 3 DIV. **M–P:** The number of neurite branches for $L1^{1152}$ mutant mice was significantly lower than that for $L1^{WT}$ mice. *, $P < 0.05$; **, $P < 0.001$. **Q–T:** The mean length or number of neurites on L1-Fc substrate was compared with the laminin substrate. Longest neurite length and neurite total length was increased more than two times, whereas number of branches of $L1^{1152}$ mice did not increase on the laminin substrate compared with $L1^{WT}$ mice. *, $P < 0.05$. Scale bar = 100 μm in D (applies to A–D) and L (applies to I–L).

and do not support L1-ankyrin playing an essential role in axonal extension or branching, as has been previously suggested (Kamiguchi and Lemmon, 2000b; Nishimura et al., 2003).

L1CD mutant mice have normal morphology and histology

All three lines of L1CD mutant mice were born in nearly Mendelian ratios of 1:3 (percentage of $L1^{mut/Y}$ mice was 29% for $L1^{Y1176A}$, 24% for $L1^{1180}$, and 22% for $L1^{1152}$), demonstrating normal survival, whereas $L1^{KO}$ was only 9%. L1CD mutant mice did not show any of the prominent features observed in $L1^{KO}$ mice, such as a domed head. The average body weights of 8-week-old $L1^{Y1176A}$ mice (26.2 ± 0.8 g; n = 8), $L1^{1180}$ mice (26.0 ± 1.1 g; n = 6), and $L1^{1152}$ mice (28.7 ± 1.0 g; n = 5) were not significantly different when compared with $L1^{WT}$ mice (25.7 ± 1.1 g; n = 6).

$L1^{KO}$ mice show gross abnormalities including hydrocephalus, smaller hippocampus and cerebellum, corpus callosum hypoplasia, hyperfasciculation, and pyramidal tract abnormalities (Dahme et al., 1997; Fransen et al., 1997; Cohen et al., 1998; Demyanenko et al., 2001; Rolf et al., 2001; Ohyama et al., 2004; Wiencken-Barger et al., 2004). To investigate whether the L1CD contributes to the defects observed in the $L1^{KO}$ mice, we examined the morphology and histology of the brains of $L1^{Y1176A}$, $L1^{1180}$, and $L1^{1152}$ mice. Because genetic background is a critical issue for brain development of $L1^{KO}$ mice (Dahme et al., 1997), we focused on the genetic background with the most severe phenotype, C57BL/6J.

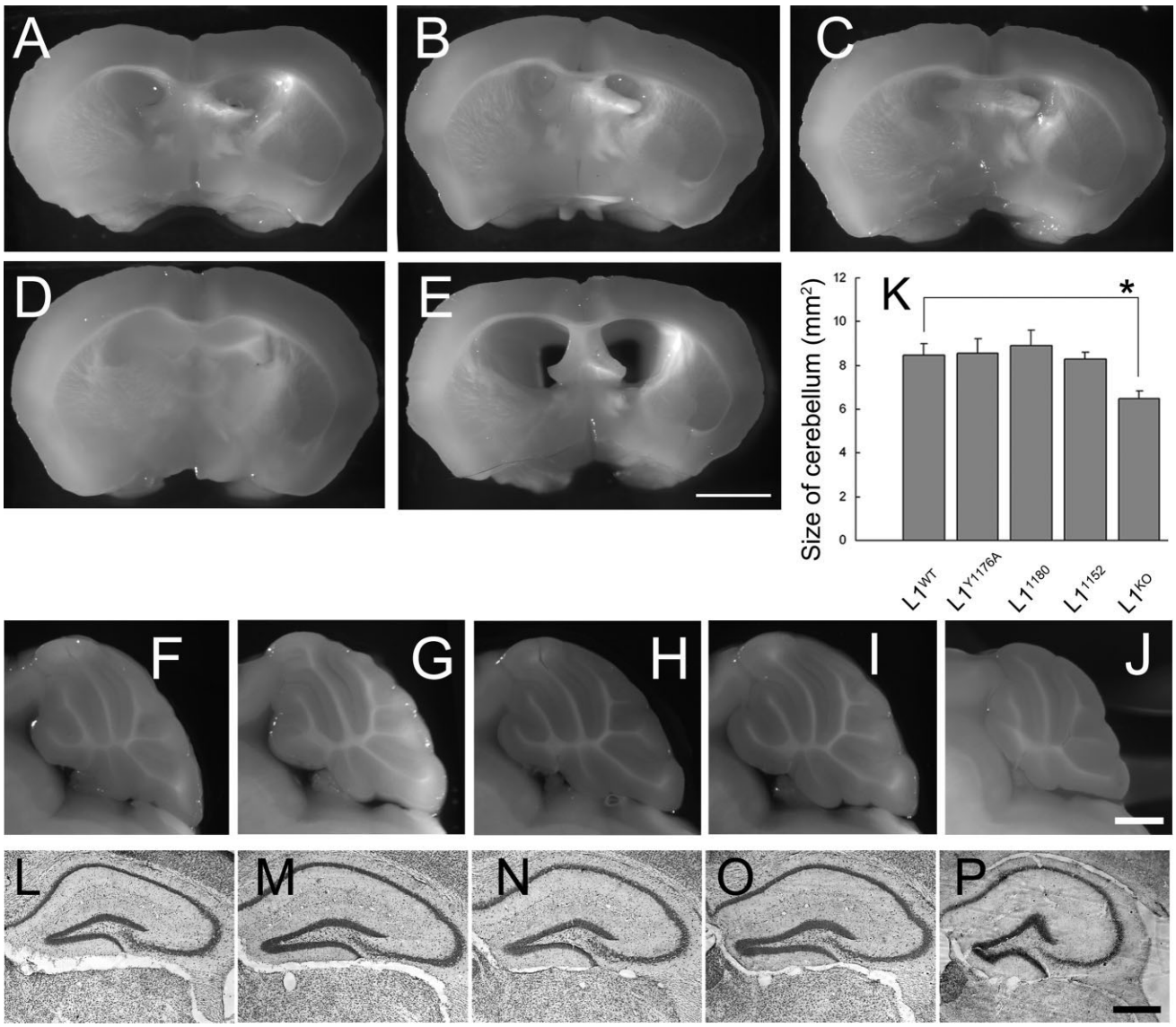

Figure 4. Lack of gross morphological abnormalities in L1CD mutant mice. A,F,L: WT. B,G,M: $L1^{Y1176A}$. C,H,N: $L1^{1180}$. D,I,O: $L1^{1152}$. E,J,P: $L1^{KO}$. **A–E:** No hydrocephalus in L1CD mutant mice. Coronal section from brains showed that there are no enlarged ventricles in L1CD mice, although $L1^{KO}$ mice have enlarged ventricles. n = 3. **F–J:** Normal morphology of cerebellar lobe in midsagittal sections of brains. The cerebellar lobule shows normal morphology in L1CD mutant mice. n = 3. **K:** Morphometric analysis of cerebellum at the midline of brains. There is no significant difference in the size of the cerebellum of L1CD mutant mice, although the $L1^{KO}$ mice cerebella are significantly smaller. n = 3. *, $P < 0.05$. **L–P:** Cresyl violet staining for hippocampus region. Formation of hippocampus is normal in L1CD mutant mice compared with $L1^{WT}$ mice, although $L1^{KO}$ mice have a smaller hippocampus. Scale bar = 200 μm in E (applies to A–E); 1 mm in J (applies to F–J); 500 μm in P (applies to L–P).

Morphologically, these three types of mutant mice showed no hydrocephalus (Fig. 4B–D); the numbers of mice with hydrocephalus were as follows: $L1^{WT}$ 0/10, $L1^{Y1176A}$ 0/9, $L1^{1180}$ 0/9, $L1^{1152}$ 0/9, and $L1^{KO}$ 5/5). In addition, no morphological abnormalities of the cerebellar lobes (Fig. 4G–I) or hippocampus (Fig. 4M–O) were observed, even though $L1^{KO}$ mice show obvious abnormalities in these brain regions (Fig. 4E,J,P). It has also been shown that $L1^{KO}$ mice sometimes have corpus callosum hypoplasia (Demyanenko et al., 2001). In contrast, these three L1CD mutant mice have corpus callosum with similar cross-sectional areas as $L1^{WT}$ mice ($L1^{WT} = 0.91 \pm 0.094$, $L1^{Y1176A} = 0.92 \pm 0.070$, $L1^{1180} = 0.85 \pm 0.070$, $L1^{1152} = 0.86 \pm 0.052$ mm^2, n = 3, $P > 0.1$).

It has previously been shown that $L1^{KO}$ mice have hyperfasciculated axons in the internal capsule (Ohyama et al., 2004; Wiencken-Barger et al., 2004). None of the three L1CD mutant mice showed hyperfasciculated axons, although all of the $L1^{KO}$ mice we examined showed hyperfasciculated axons instead of the

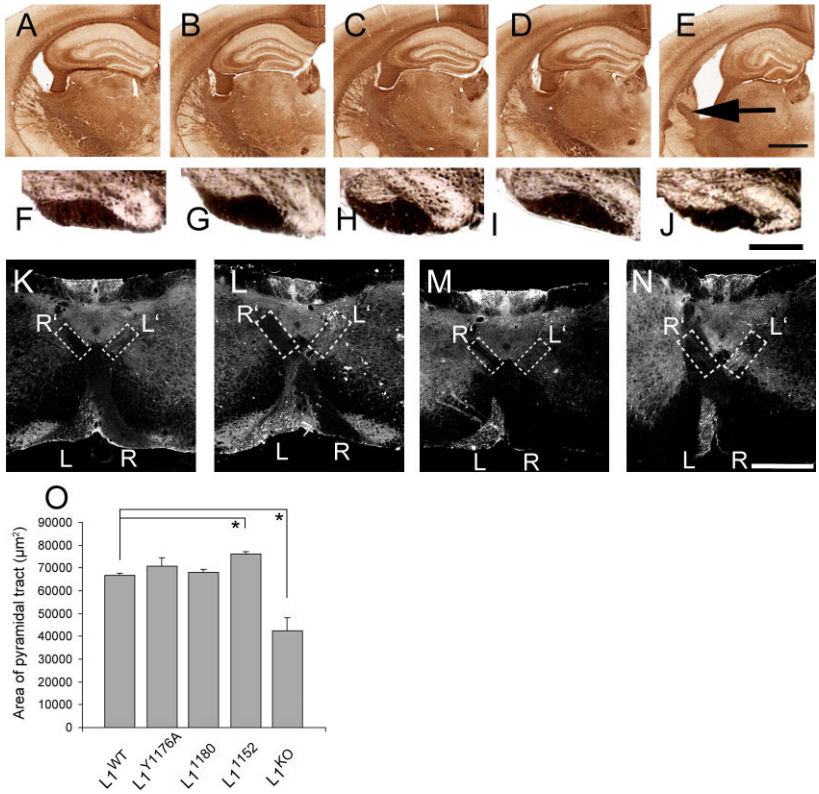

Figure 5. Normal axonal guidance in L1CD mutant mice. A,F,K: WT. B,G,L: $L1^{Y1176A}$. C,H,M: $L1^{I180}$. D,I,N: $L1^{I152}$. E,J: $L1^{KO}$. **A-E:** Neurofilament staining of brain sections. There is no hyperfasciculation of axons in the internal capsule of L1CD mice, although $L1^{KO}$ mice have hyperfasciculated axons (arrow). **F–J:** Coronal sections in medulla of adult mice. The morphology of the pyramidal tract is normal in L1CD mutant mice compared with $L1^{WT}$ mice. **O:** The size of the pyramidal tract was not significantly different between all L1CD mutant mice and $L1^{WT}$ mice, although $L1^{KO}$ mice have significantly smaller pyramidal tracts. n = 3. *, $P < 0.005$. **K–N:** The pyramidal tract is normal in L1CD mutant mice. BDA was injected into the left side of the motor cortex. At the pyramidal decussation area, the labeled pyramidal tract was observed in the left side of the ventral region (L) and also in the contralateral side of the dorsal region (L′) in all L1CD mice and $L1^{WT}$ mice. In contrast, the dorsal ipsilateral pyramidal tracts are not labeled. Scale bar = 1 mm in E (applies to A–E); 300 μm in J (applies to F–J); 500 μm in N (applies to K–N).

many small axon bundles characteristic of wild-type animals (Fig. 5A–E). Preliminary studies did not detect decreased sizes of the thalamus in the L1CD mice (data not shown).

Corticospinal tract (CST) axons of $L1^{KO}$ mice often display pathfinding errors at the pyramidal decussation, and the cross-sectional area of the corticospinal tract is significantly decreased (Dahme et al., 1997; Cohen et al., 1998). To evaluate whether similar abnormalities occurred in L1CD mice, we determined the area of the CST at the caudal end of the medulla (Fig. 5F–J). The area was almost identical between $L1^{WT}$ and L1CD mice, although $L1^{KO}$ mice showed a significantly smaller area (Fig. 5O). The CST was anterogradely labeled by BDA from a unilateral injection in the motor cortex. The labeled axons in the CST were observed coursing contralaterally in the ventral region in the pyramidal decussation area, with no axons going into the ipsilateral CST (Fig. 5K–N), indicating that the pyramidal decussation occurred normally in all L1CD mutant mice, even though $L1^{KO}$ mice showed pathfinding errors (Dahme et al., 1997; Cohen et al., 1998; Itoh et al., 2004).

These data show that common and easily identifiable abnormities observed in $L1^{KO}$ mice were not found in mice with L1CD mutations.

Normal spatial memory

It has previously been reported that the $L1^{KO}$ mice have defects in spatial learning and memory as assessed with the Morris water maze (Fransen et al., 1998). To examine spatial learning and memory, we performed the radial arm water maze test (Alamed et al., 2006). The average time to reach the platform was not different between L1CD mutant mice and $L1^{WT}$ mice (Fig. 6A). To exclude the possibility that the mouse found the platform by randomly swimming around, we counted how many times a mouse entered the wrong arm. We found no significant difference in the number of errors between L1CD mutant lines and $L1^{WT}$ mice (Fig. 6B). These data indicate that the L1CD is

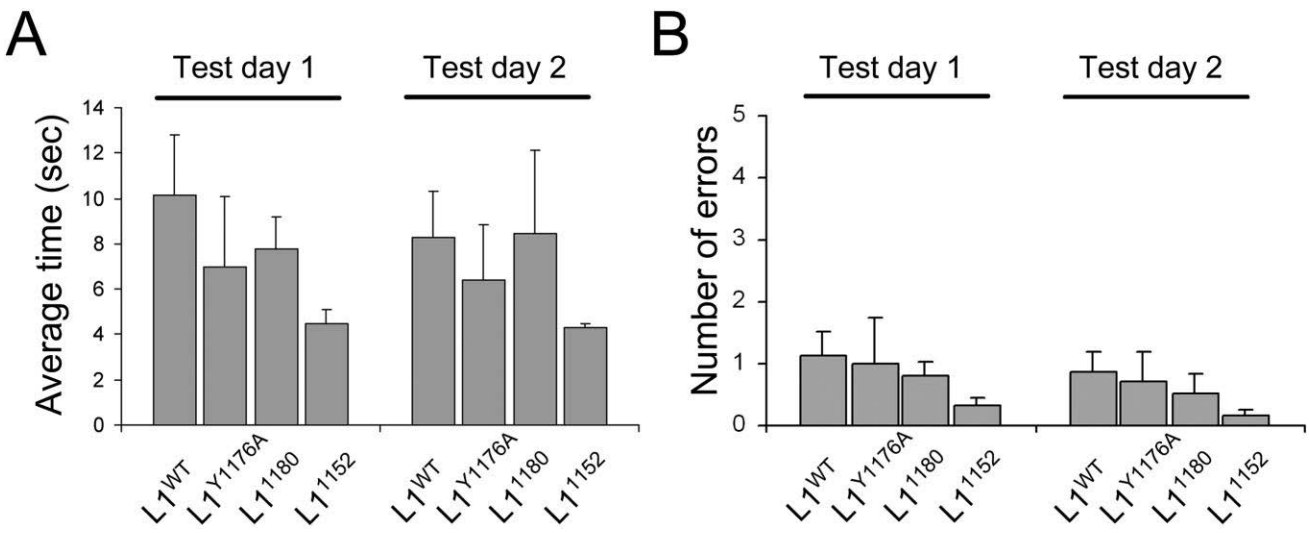

Figure 6. Normal spatial memory in L1CD mutant mice. Radial-arm water maze for spatial memory. **A,B:** The average time for finding the platform (A) and the average number of errors (B) were not significantly different between L1CD mutant mice and $L1^{WT}$ mice. $L1^{WT}$, n = 7; $L1^{Y1176A}$, n = 4; $L1^{1180}$, n = 7; $L1^{1152}$, n = 6.

not essential for spatial learning and memory. It was noted that the L1CD mutant mice, especially the 1152 mutants, actually had "better performance" on the radial arm water maze, in terms of having shorter times to swim to the platform, although this was not statistically significant. Observations from the tests indicate that the shorter latency was likely due to less time spent floating in the water before starting to swim to the platform. It is possible that this is due to some difference in anxiety levels in the L1CD mice (Venero et al., 2004).

Truncations of the L1CD lead to impaired motor function

It has been shown that $L1^{KO}$ mice fall easily from an immobile rod because of difficulties in keeping their balance (Fransen et al., 1998); however, we found that L1CD mutant mice can stay on an immobile rod without falling. To further examine motor function and coordination of L1CD mutant mice, we performed the accelerated rotarod test to examine their ability to remain on a rotating platform (Pratte et al., 2003). There was no significant difference between the times of $L1^{Y1176A}$ and $L1^{WT}$ mice; however, the $L1^{1180}$ and $L1^{1152}$ mice performed worse (Fig. 7). The difference in performance of the WT mice used in different experimental series (compare Fig. 7B with A or C) is due to different ages of the WT and aged-matched L1CD mice: Fig. 7A, 2 months; Fig. 7B, 7–8 months; Fig. 7C,: 2–4 months). These data indicate that the C-terminal region of the L1CD, including the ankyrin-binding region, is important in motor function in the adult mouse.

L1CD mutant mice have normal unmyelinated and myelinated axons

Although the cerebellum is a region of the brain that plays an important role in motor control, all L1CD mutant mice, including $L1^{1152}$, did not show detectable abnormalities in cerebellum formation (Fig. 4). The development of myelinated and unmyelinated axons in the PNS is also important for motor function. To examine this issue, we used light and electron microscopic techniques. In the sciatic nerve of $L1^{WT}$ mice, Schwann cells ensheathe individual axons compactly within separate cytoplasmic processes (Fig. 8A). In L1CD mutant mice (Fig. 8C–E), these axons were also compactly ensheathed, similar to $L1^{WT}$ mice (Fig. 8A). This is in contrast to $L1^{KO}$ mice (Fig. 8B) and mice lacking the L1 6th Ig domain (L1-6D mice), in which there are many unmyelinated axons not properly ensheathed by Schwann cell processes (Dahme et al., 1997; Haney et al., 1999; Itoh et al., 2005). To quantify this, we categorized ensheathment into three types; not ensheathed, partially ensheathed, and completely ensheathed (Fig. 8F,G). In L1CD mutant mice, the Schwann cells processes wrap each axon similar to $L1^{WT}$ mice, in contrast to $L1^{KO}$ mice (Fig. 8H).

Next we examined the ultrastructure of myelinated axons. Myelin membranes were tightly packed, and the periaxonal space was appropriately maintained in L1CD mice (Fig. 8C–E). We analyzed the myelinated axons in the entire cross-sectional area of nerves from four $L1^{WT}$ mice and from four of each L1CD mutant mice; about 2,500 axons per animal were measured. The g-ratio is the accepted

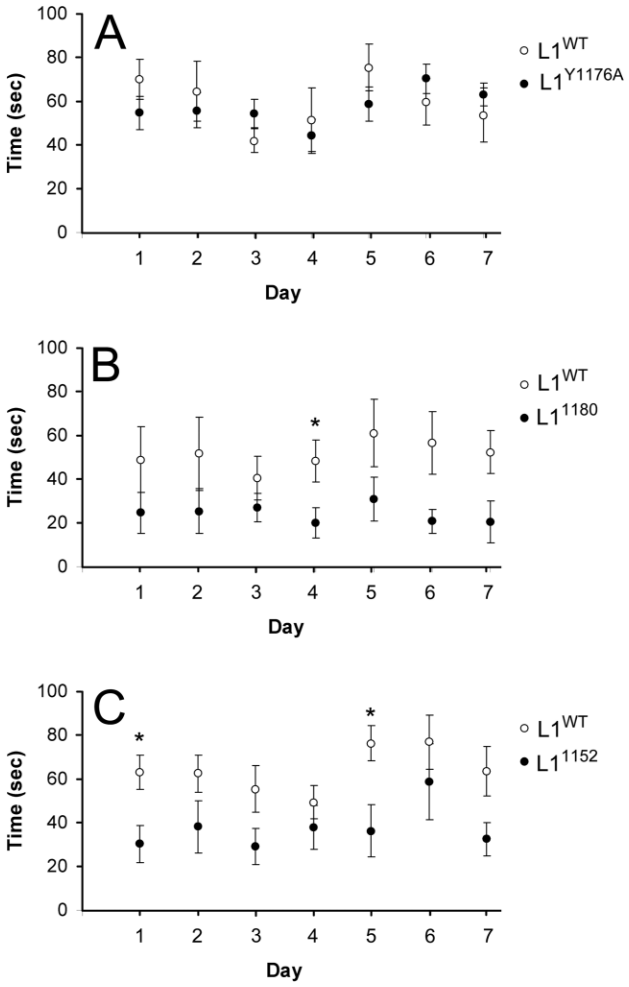

Figure 7. Impaired motor function in $L1^{1180}$ and $L1^{1152}$ mice. The time in balance on the accelerated rotarod was measured by using age-matched mice, comparing the L1CD mutant mice and $L1^{WT}$ mice. $L1^{1180}$ (**B**) and $L1^{1152}$ (**C**) mutant mice showed a significantly reduced performance compared with $L1^{WT}$ mice, but the $L1^{Y1176A}$ mice (**A**) did not. $L1^{WT}$, n = 8; $L1^{Y1176A}$, n = 7; $L1^{1180}$, n = 7; $L1^{1152}$, n = 7; $*P < 0.05$.

measurement for the thickness of myelin sheaths. The average g-ratio was not significantly different between $L1^{WT}$ and L1CD mutant mice (Fig. 8I). The population distribution of g-ratios did not show significant differences between $L1^{WT}$ and L1CD mutant mice (Fig. 8J–L), although the g-ratio of $L1^{KO}$ mice (Fig. 8M) was significantly larger than $L1^{WT}$ ($P < 0.005$), indicating that myelin is thinner in $L1^{KO}$ mice than $L1^{WT}$ mice. These results show that the development of unmyelinated and myelinated PNS axons is normal in L1CD mutant mice.

L1 protein expression decreases with age in L1CD mutant mice

We did not detect any gross morphological or histological abnormalities in the CNS and PNS, although $L1^{1180}$ and $L1^{1152}$ mice exhibited defects in motor function, possibly due to the fact that these two mutant lines do not have Ank2 binding sites. It has been demonstrated that Ank2 binding mediates stationary behavior of L1 (Garver et al., 1997; Scotland et al., 1998; Gil et al., 2003). Although all of the L1CD mutant lines express L1 protein in axons of young hippocampal neurons in vitro, we examined the localization of L1 in the brains of mutant mice at postnatal day 7 (P7) and in 7-week-old mice. At P7, there is no obvious difference in the localization of L1 between $L1^{WT}$ and L1CD mutant mice using the L1ex antibody (Fig. 9A–D). Of particular note, there is no accumulation of L1 in cell bodies of the sort observed in C264Y (Runker et al., 2003), which confirms that the L1CD lines with these particular mutations/truncations can be transported from the cell body to the axon.

However, the quantitative data for the expression level of L1 protein at P7 showed that the amount of L1 protein present in the brain was reduced by about 50% in $L1^{1180}$ and $L1^{1152}$ mice compared with $L1^{WT}$ (Fig. 9E–F). The reduction of L1 protein was much more prominent in 7-week-old mice with L1CD truncations. $L1^{WT}$ mice and $L1^{Y1176A}$ mutant mice had prominent and similarly distributed L1 immunoreactivity in the hippocampus and in the molecular layer of the cerebellar cortex. In contrast, $L1^{1180}$ and $L1^{1152}$ mice showed faint or no L1 immunoreactivity. Other regions where L1 expression is high in the adult, including the stria terminalis, fimbria, and hypothalamus (Munakata et al., 2003), also showed only faint or no L1 immunoreactivity (data not shown). Furthermore, Western blot analysis also demonstrated a significant reduction in the level of L1 protein in $L1^{1180}$ and $L1^{1152}$ mice (Fig. 9O–P), whereas there was no significant difference in the expression level of L1 mRNA (Fig. 9Q). These data suggest that the L1CD, C-terminal to the RSLE mini-exon, is required for the persistent expression of L1 protein after early developmental stages.

DISCUSSION

These three L1cam mutant mice lines are novel models for studying the highly conserved L1CD (Hortsch, 1996). A variety of cell biological, biochemical, and molecular experiments have shown that the L1CD has important binding partners involved in signaling, trafficking, and cytoskeletal interactions (Kamiguchi and Lemmon, 2000a; Maness and Schachner, 2007). Mutations in the L1CD cause a form of mental retardation, although not as devastating as mutations in the L1 extracellular domain (L1ED) (Yamasaki et al., 1997). Therefore, it is remarkable that after examining a wide range of features of the CNS and PNS in the L1CD mice, we conclude that the L1CD is not responsible for the large anatomical defects observed in the $L1^{KO}$ mice. However, the L1CD is essential for the persistent

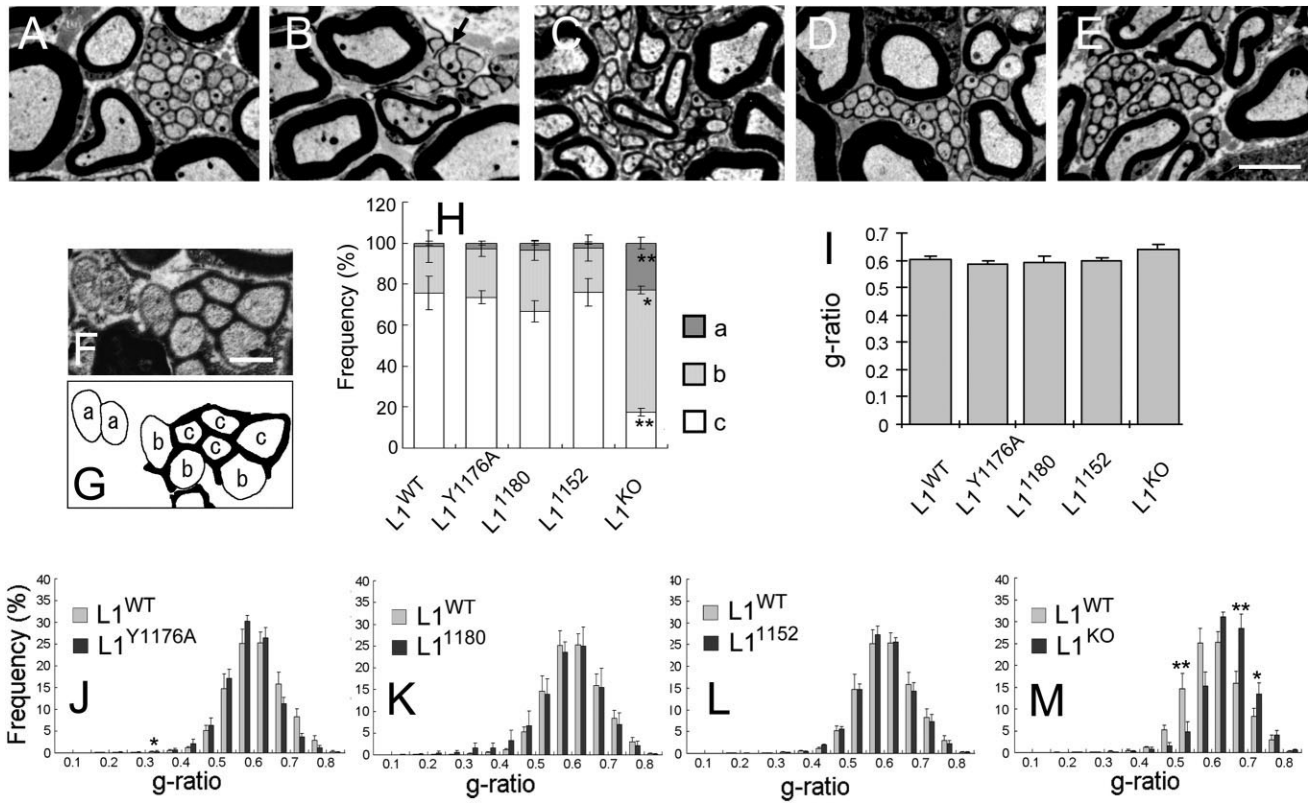

Figure 8. Normal morphology of unmyelinated and myelinated axons. Electron microscopy of sciatic nerves of 8-week-old mice A: $L1^{WT}$. B: $L1^{KO}$. C: $L1^{Y1176A}$. D: $L1^{1180}$. E: $L1^{1152}$. **A–E:** Schwann cells compactly ensheathe multiple unmyelinated axons in $L1^{WT}$ and in all L1CD mutant mice, although $L1^{KO}$ showed abnormal Remak bundles. Myelin membranes were tightly packed around large axons in $L1^{WT}$ and in all L1CD mutant mice. **F,G:** Classification scheme of unmyelinated axons depending on the degree of ensheathment. a, not ensheathed; b, partially ensheathed; c, completely ensheathed. **H:** The percentage of completely ensheathed unmyelinated axons was almost identical between L1CD mutant mice and $L1^{WT}$ mice, whereas it was significantly reduced in $L1^{KO}$ mice. *, $P < 0.01$; **, $P < 0.005$. **I:** g-ratio averages. There is no significant difference in the average g-ratio of L1CD mice compared with $L1^{WT}$ mice. **J–M:** Distribution of g-ratios. There is no significant difference in the distribution of g-ratios in L1CD mice compared with $L1^{WT}$ mice, although $L1^{KO}$ mice have a larger proportion of axons with large g-ratios. *, $P < 0.05$; **, $P < 0.01$. Scale bar = 3 μm in E (applies to A–E), = 1 μmin F.

expression of L1 protein and for some aspect of motor coordination.

Several binding partners for the L1CD have been found, including AP-2, ERM, RanBPM, and Ank2. The interaction with AP-2 enables L1 endocytosis via clathrin-coated pits, and it also is involved in axonal sorting (Kamiguchi and Lemmon, 1998; Kamiguchi et al., 1998b; Wisco et al., 2003). Based on these in vitro experiments, it seemed likely that L1 transportation from the cell body to the axon might be disturbed, but the data from our in vitro and vivo analysis showed that the distribution of L1 in the brain appears normal at P7, even if the L1CD was almost entirely missing. Winckler and associates have published a series of in vitro studies on the sorting of the chicken homologue of L1, called Ng-CAM, into somatodendritic and axonal compartments in neurons (Wisco et al., 2003; Yap et al., 2008). They have found that the tyrosine-based signal is important for retrieval of Ng-CAM from the somatodendritic compartment prior to transport into the axon but that direct trafficking to the axon is also possible using a signal in the L1ED (Wisco et al., 2003). Sampo et al. (2003) have come to similar conclusions. Although the extracellular domains of L1 and NgCAM are substantially different, the present studies also show that L1 sorting into the axon does not require the L1CD.

Humans with extracellular domain mutations or truncations usually have defects in the development of the corticospinal tract (Halliday et al., 1986). Similarly, $L1^{KO}$ mice often have corticospinal tract defects, including abnormal decussation (Cohen et al., 1998). This abnormal pathfinding is attributed to a loss of the L1-neuropilin-1 interactions that mediate Sema3A signaling (Castellani, 2002; Castellani et al., 2000, 2002). It is well established that L1 and neuropilin-1 bind to each other via their extracellular domains (Castellani et al., 2000; Castellani et al., 2002). Recently, it has been reported that L1-ERM interactions

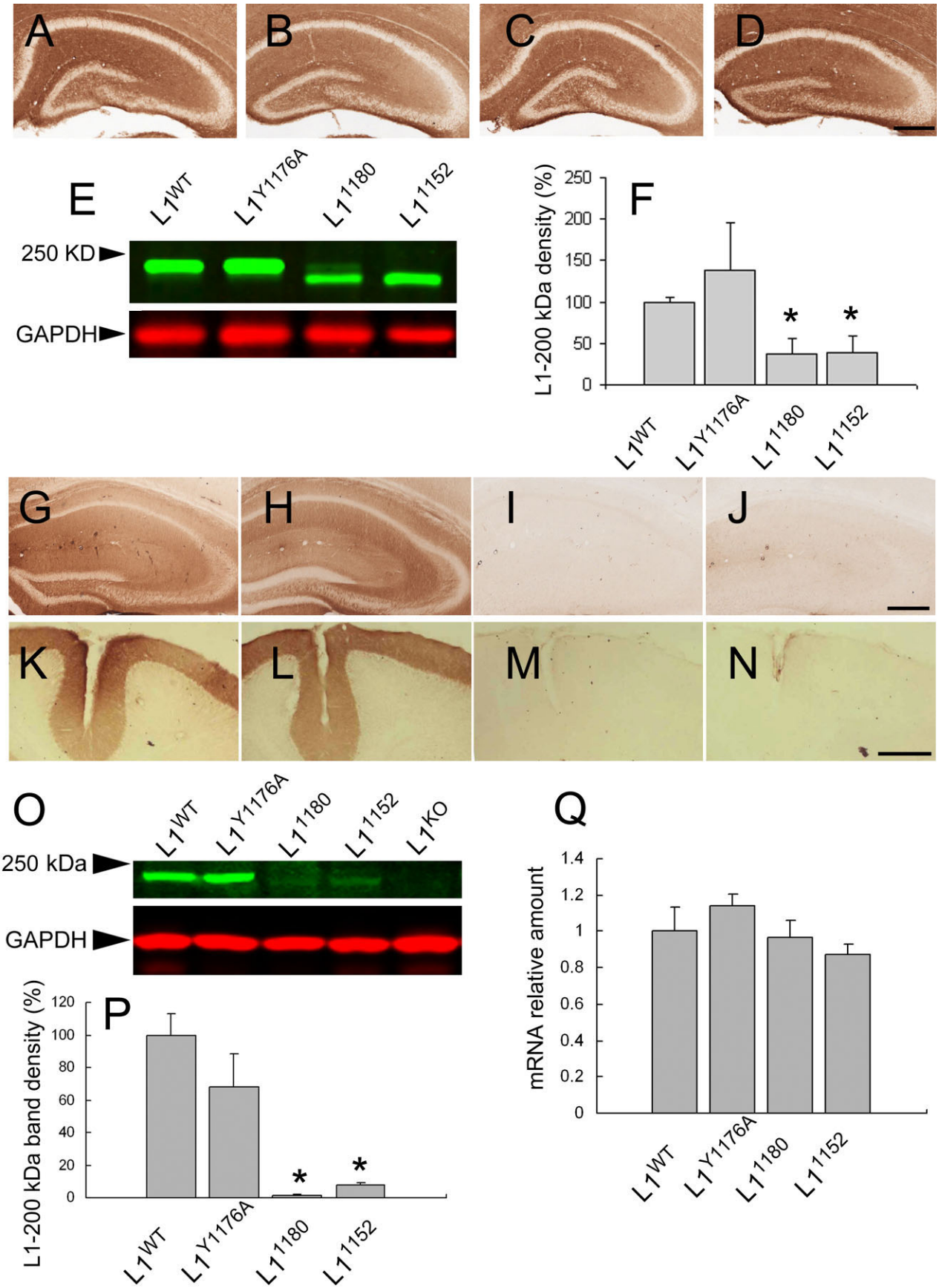
A
B
C
D
E
L1WT
L1Y1176A
L11180
L11152
250 KD
GAPDH
F
L1-200 kDa density (%)
250
200
150
100
50
0
*
*
L1WT
L1Y1176A
L11180
L11152
G
H
I
J
K
L
M
N
O
L1WT
L1Y1176A
L11180
L11152
L1KO
250 kDa
GAPDH
P
L1-200 kDa band density (%)
120
100
80
60
40
20
0
*
*
L1WT
L1Y1176A
L11180
L11152
Q
mRNA relative amount
1.4
1.2
1
0.8
0.6
0.4
0.2
0
L1WT
L1Y1176A
L11180
L11152

Figure 9

can mediate both L1/neuropilin-1 internalization and Sema3A-induced growth cone collapse (Mintz et al., 2008). However, it is clear that the $L1^{Y1176A}$ and the $L1^{1152}$ mice do not depend on L1-ERM or L1-AP-2 interactions to send axons correctly along the corticospinal tract. This would argue that the L1-dependent Sema3A response that subserves decussation of the corticospinal tract is not dependent on AP-2-or ERM-mediated internalization of L1/neuropilin-1 complexes.

Perhaps the most important finding in the present work is that the persistent expression of L1 protein is not required for the maintenance of normal brain morphology or cytoarchitecture or learning and memory assessed by the radial arm water maze. The amount of L1 protein decreases to barely detectable levels in adult mice lacking the C-terminal portion of the L1CD ($L1^{1152}$ or $L1^{1180}$ mutant mice) and is even reduced by approximately 50% at P7. There is no doubt that L1 is essential for axonal growth and pathfinding as well as proper brain formation, because the $L1^{KO}$ mice show a variety of morphological abnormalities (Dahme et al., 1997; Cohen et al., 1998; Fransen et al., 1998; Rolf et al., 2001; Ohyama et al., 2004; Wiencken-Barger et al., 2004). Although there is some variation depending on brain region, L1 is expressed at relatively high levels during development and L1 expression decreases somewhat (on average by perhaps 50%) in the adult (Liljelund et al., 1994). The continued expression of L1 in brain regions with substantial neuronal plasticity (the hippocampus and cerebellum, for example), would seem to argue for an important role for L1 in adult. Indeed L1 has been implicated in some models of learning (Fransen et al., 1998; Wolfer et al., 1998; Law et al., 2003; Venero et al., 2004), and in synapse formation (Godenschwege et al., 2006; Triana-Baltzer et al., 2008).

The data from the $L1^{1152}$ and $L1^{1180}$ mice allow us to disassociate the effects of loss of L1 function in development from loss of function in the adult. In the adult, after brain formation is complete, if L1 is then lost, it is difficult to find effects on brain morphology, cytoarchitecture, axonal pathfinding, or learning and memory. The only significant alteration we observed was in motor function.

In humans, mutations of the L1CAM gene usually cause spastic paraplegia and adducted thumbs. Adducted thumbs are typically present at birth and might be due to failure of innervation of the adductors in the forearm (Holtzman et al., 1976; Kanemura et al., 2006). Macias et al. found the human mutation (S1181X) that causes the truncation of L1 protein, similar to our $L1^{1180}$ mice (Macias et al., 1992; Weller and Gartner, 2001). This human mutation did not cause hydrocephalus or corpus callosum hypoplasia, but it did cause spastic paraplegia and adducted thumbs. Kanemura et al. (2005) reported a MASA syndrome case with a truncation at R1166X in exon 27 that is similar to our L1-1552 mouse line. The individual had shuffling gate and adducted thumbs, but MRI revealed a relatively normal brain; in particular, no abnormalities in the brainstem or cerebellum were noted. These defects in motor function in humans with truncations in the L1CD could result from similar failures as those observed in our two truncated L1CD mutant mice, so it is plausible that stable expression of L1 in the adult is essential for normal function of the motor system. The root cause of the abnormal motor function in the $L1^{1180}$ and $L1^{1152}$ mutant mice is not apparent. One possible site of action could be the synapse. Perhaps some aspect of CNS circuitry in the motor system is abnormal but undetected with the methods we used in our survey of brain formation. Alternatively, the site of action could be in the PNS at the neuromuscular junction. It has been shown that L1 is present presynaptically and disruption of L1 function alters neuromuscular junction formation (Triana-Baltzer et al., 2006).

Which region of the L1CD determines the stability of L1 protein in the adult? The decrease of L1 protein was observed only in $L1^{1180}$ and $L1^{1152}$ mice but not in $L1^{Y1176A}$ mutant mice. The two affected mutant lines both lack the region C-terminal to residue 1180, therefore missing the Ank2 and RanBPM binding sites (Davis and Bennett, 1994; Cheng et al., 2005b; Whittard et al., 2006). It has been

Figure 9. Expression level of L1 mRNA is normal, but L1 protein expression is dramatically reduced in 7-week-old mice with truncations that remove the ankyrin-binding site. L1 protein localization using L1ex antibody in hippocampus in postnatal day 7 mice A: $L1^{WT}$. B: $L1^{Y1176A}$. C: $L1^{1180}$. D: $L1^{1152}$. **A–D:** All L1CD mutant mice show similar distribution of L1 in the hippocampus. **E:** Western blot analysis of L1 protein in postnatal day 7 mice using L1ex monoclonal antibody. All L1CD mutant mice showed L1 bands, although the band density was a lower in $L1^{1180}$ and $L1^{1152}$ mice compared with $L1^{WT}$ mice. The lower (red) panel shows the GAPDH loading control. **F:** Relative amount of L1-200-kDa band density normalized to GAPDH loading control. n = 3.*, $P < 0.05$. **G–N:** L1 protein localization using L1ex monoclonal antibody in the hippocampus (G: $L1^{WT}$. H: $L1^{Y1176A}$. I: $L1^{1180}$. J: $L1^{1152}$) and cerebellum (K: $L1^{WT}$. L: $L1^{Y1176A}$. M: $L1^{1180}$. N: $L1^{1152}$) in 7-week-old mice. There was almost no L1 in the hippocampus and cerebellum of $L1^{1180}$ and $L1^{1152}$ mice, although $L1^{Y1176A}$ mice have similar expression patterns to $L1^{WT}$ mice. **O:** Western blot analysis of L1 protein in 7-week-old mice. The L1 band was detected by L1ex antibody in L1CD mice, although there was no band in $L1^{KO}$ mice. The band density of $L1^{1180}$ and $L1^{1152}$ was obviously weaker than $L1^{WT}$ and $L1^{Y1176A}$ mice. The lower (red) band is the GAPDH loading control. **P:** Relative amount of L1-200-kDa band density, which is normalized to the GAPDH loading control. The band density was significantly lower in $L1^{1180}$ and $L1^{1152}$ mice compared with $L1^{WT}$ mice. $L1^{WT}$, n = 3; $L1^{Y1176A}$, n = 3; $L1^{1180}$, n = 3; $L1^{1152}$, n = 3. *$P < 0.01$. **Q:** Quantitative analysis of L1 mRNA in 7-week-old mice. The L1 mRNA relative amount, normalized to β-actin, showed no significant difference in L1CD mutant mice compared with $L1^{WT}$ mice. $L1^{WT}$, n = 3; $L1^{Y1176A}$, n = 3; $L1^{1180}$, n = 3; $L1^{1152}$, n = 3. Scale bar = 300 μm in D (applies to A–D), J (applies to G–J), and N (applies to K–N).

suggested that L1-ERM interactions predominate early in development but that L1-ankyrin interactions dominate at later developmental stages and in the adult (Mintz et al., 2003; Hortsch et al., 2009). Interestingly, in the Ank2 knockout mice, L1 expression is dramatically affected, with almost a complete loss of L1 in brain sections and the optic nerve at P7 (Scotland et al., 1998). Recently, Buhusi et al. (2008) described a mouse line with a point mutation in the L1CD (Y1229H) that disrupts L1-Ank2 interactions. They reported that L1 was expressed at normal levels in the P0 and P3 brain, but the levels in the adult brain were not reported. No abnormalities in brain morphology were noted, but a subtle defect in targeting of some retinal axons to the tectum was reported in P10–12 mice. When these data are taken together, it is likely that the loss of L1-Ank2 interactions accounts for the loss of L1 expression in the adult in our mice.

Although our previous data showed that L1-mediated neurite branching was regulated by two ERM binding sites, the mutation of the juxtamembrane ERM site showed the strongest effect on neurite branching (Cheng et al., 2005a). This paper shows that L1-mediated neurite branching is strongly decreased in $L1^{1152}$ mice, but not in $L1^{Y1176A}$ or $L1^{1180}$ mice. These data suggest that the juxtamembrane ERM binding site is essential for L1-mediated neurite branching, although we did not observe axon branching or corticospinal tract guidance abnormalities in vivo.

The highly conserved nature of the L1CD (it is completely conserved in mammals at the amino acid level) is prima facie evidence that it plays an essential role in L1cam function. The fact that so many obvious defects present in the $L1^{KO}$ mice were absent in the L1CD mice indicates the likely presence of some compensatory mechanisms ameliorating the affects that might be expected, especially in signaling and axon guidance. One possibility is that other L1 family members are serving a compensatory role. Neurofascin, Nr-CAM, and CHL1 all have cytoplasmic domains that are highly homologous to the L1CD (Hortsch, 2000). They all have the RSLE mini-exon, ankyrin binding regions, and a highly conserved juxtamembrane region. An argument in favor of this possibility is the fact that both the L1 and NrCAM knockouts have mild effects on the cerebellum but the double knockout has a very severe effect on cerebellar development (Sakurai et al., 2001) and the double knockouts are much smaller and show lower survival rates than the single knockouts. Alternatively (or perhaps in addition to other L1cam family members), signaling via the epidermal growth factor (EGF) or fibroblast growth factor (FGF) receptors (Chen et al., 2001; Islam et al., 2004; Kulahin et al., 2008), TAG-1 family members (Felsenfeld et al., 1994; Pavlou et al., 2002), or neuropilin (Castellani et al., 2002) could compensate for some loss of signaling via the L1CD

In summary, although the L1 cytoplasmic domain is very highly conserved over evolution, the loss of the L1 cytoplasmic domain appears to have only minor effects on altering brain structure and function in mice. This is in stark contrast to the role of the L1 extracellular domain, which is essential for a variety of critical processes in brain development.

ACKNOWLEDGMENTS

We thank S. O'Gorman for helping to make the L1CD mutant mice and H. Kamiguchi for discussions. We also thank F. Rathjen and M.N. Rasband for supplying antibodies. V. Lemmon holds the Walter G. Ross Distinguished Chair in Developmental Neuroscience at the University of Miami.

LITERATURE CITED

Alamed J, Wilcock DM, Diamond DM, Gordon MN, Morgan D. 2006. Two-day radial-arm water maze learning and memory task; robust resolution of amyloid-related memory deficits in transgenic mice. Nat Protoc 1:1671–1679.

Barbin G, Aigrot MS, Charles P, Foucher A, Grumet M, Schachner M, Zalc B, Lubetzki C. 2004. Axonal cell-adhesion molecule L1 in CNS myelination. Neuron Glia Biol 1:65–72.

Brittis PA, Lemmon V, Rutishauser U, Silver J. 1995. Unique changes of ganglion cell growth cone behavior following cell adhesion molecule perturbations: a time-lapse study of the living retina. Mol Cell Neurosci 6:433–449.

Buhusi M, Schlatter MC, Demyanenko GP, Thresher R, Maness PF. 2008. L1 interaction with ankyrin regulates mediolateral topography in the retinocollicular projection. J Neurosci 28: 177–188.

Castellani V. 2002. The function of neuropilin/L1 complex. Adv Exp Med Biol 515:91–102.

Castellani V, Chedotal A, Schachner M, Faivre-Sarrailh C, Rougon G. 2000. Analysis of the L1-deficient mouse phenotype reveals cross-talk between Sema3A and L1 signaling pathways in axonal guidance. Neuron 27:237–249.

Castellani V, De Angelis E, Kenwrick S, Rougon G. 2002. Cis and trans interactions of L1 with neuropilin-1 control axonal responses to semaphorin 3A. EMBO J 21:6348–6357.

Chen L, Ong B, Bennett V. 2001. LAD-1, the *Caenorhabditis elegans* L1CAM homologue, participates in embryonic and gonadal morphogenesis and is a substrate for fibroblast growth factor receptor pathway-dependent phosphotyrosine-based signaling. J Cell Biol 154:841–855.

Cheng L, Itoh K, Lemmon V. 2005a. L1-mediated branching is regulated by two ezrin-radixin-moesin (ERM)-binding sites, the RSLE region and a novel juxtamembrane ERM-binding region. J Neurosci 25:395–403.

Cheng L, Lemmon S, Lemmon V. 2005b. RanBPM is an L1-interacting protein that regulates L1-mediated mitogen-activated protein kinase activation. J Neurochem 94:1102–1110.

Cohen NR, Taylor JS, Scott LB, Guillery RW, Soriano P, Furley AJ. 1998. Errors in corticospinal axon guidance in mice lacking the neural cell adhesion molecule L1. Curr Biol 8:26–33.

Dahme M, Bartsch U, Martini R, Anliker B, Schachner M, Mantei N. 1997. Disruption of the mouse L1 gene leads to malformations of the nervous system. Nat Genet 17:346–349.

Davis JQ, Bennett V. 1994. Ankyrin binding activity shared by the neurofascin/L1/NrCAM family of nervous system cell adhesion molecules. J Biol Chem 269:27163–27166.

Demyanenko GP, Shibata Y, Maness PF. 2001. Altered distribution of dopaminergic neurons in the brain of L1 null mice. Brain Res Dev Brain Res 126:21–30.

Dequidt C, Danglot L, Alberts P, Galli T, Choquet D, Thoumine O. 2007. Fast turnover of L1 adhesions in neuronal growth cones involving both surface diffusion and exo/endocytosis of L1 molecules. Mol Biol Cell 18:3131–3143.

Dickson TC, Mintz CD, Benson DL, Salton SR. 2002. Functional binding interaction identified between the axonal CAM L1 and members of the ERM family. J Cell Biol 157:1105–1112.

Dotti CG, Banker GA, Binder LI. 1987. The expression and distribution of the microtubule-associated proteins tau and microtubule-associated protein 2 in hippocampal neurons in the rat in situ and in cell culture. Neuroscience 23:121–130.

Felsenfeld DP, Hynes MA, Skoler KM, Furley AJ, Jessell TM. 1994. TAG-1 can mediate homophilic binding, but neurite outgrowth on TAG-1 requires an L1-like molecule and beta 1 integrins. Neuron 12:675–690.

Fransen E, Van Camp G, Vits L, Willems PJ. 1997. L1-associated diseases: clinical geneticists divide, molecular geneticists unite. Hum Mol Genet 6:1625–1632.

Fransen E, D'Hooge R, Van Camp G, Verhoye M, Sijbers J, Reyniers E, Soriano P, Kamiguchi H, Willemsen R, Koekkoek SK, De Zeeuw CI, De Deyn PP, Van der Linden A, Lemmon V, Kooy RF, Willems PJ. 1998. L1 knockout mice show dilated ventricles, vermis hypoplasia and impaired exploration patterns. Hum Mol Genet 7:999–1009.

Garver TD, Ren Q, Tuvia S, Bennett V. 1997. Tyrosine phosphorylation at a site highly conserved in the L1 family of cell adhesion molecules abolishes ankyrin binding and increases lateral mobility of neurofascin. J Cell Biol 137:703–714.

Gil OD, Sakurai T, Bradley AE, Fink MY, Cassella MR, Kuo JA, Felsenfeld DP. 2003. Ankyrin binding mediates L1CAM interactions with static components of the cytoskeleton and inhibits retrograde movement of L1CAM on the cell surface. J Cell Biol 162:719–730.

Godenschwege TA, Kristiansen LV, Uthaman SB, Hortsch M, Murphey RK. 2006. A conserved role for *Drosophila* Neuroglian and human L1-CAM in central-synapse formation. Curr Biol 16:12–23.

Grumet M, Edelman GM. 1988. Neuron-glia cell adhesion molecule interacts with neurons and astroglia via different binding mechanisms. J Cell Biol 106:487–503.

Grumet M, Friedlander DR, Edelman GM. 1993. Evidence for the binding of Ng-CAM to laminin. Cell Adhes Commun 1:177–190.

Halliday J, Chow CW, Wallace D, Danks DM. 1986. X linked hydrocephalus: a survey of a 20 year period in Victoria, Australia. J Med Genet 23:23–31.

Haney CA, Sahenk Z, Li C, Lemmon VP, Roder J, Trapp BD. 1999. Heterophilic binding of L1 on unmyelinated sensory axons mediates Schwann cell adhesion and is required for axonal survival. J Cell Biol 146:1173–1184.

Haspel J, Grumet M. 2003. The L1CAM extracellular region: a multi-domain protein with modular and cooperative binding modes. Front Biosci 8:s1210–1225.

Holtzman RN, Garcia L, Koenigsberger R. 1976. Hydrocephalus and congenital clasped thumbs: a case report with electromyographic evaluation. Dev Med Child Neurol 18:521–524.

Hortsch M. 1996. The L1 family of neural cell adhesion molecules: old proteins performing new tricks. Neuron 17:587–593.

Hortsch M. 2000. Structural and functional evolution of the L1 family: are four adhesion molecules better than one? Mol Cell Neurosci 15:1–10.

Hortsch M, Nagaraj K, Godenschwege TA. 2009. The interaction between L1-type proteins and ankyrins—a master switch for L1-type CAM function. Cell Mol Biol Lett 14:57–69.

Islam R, Kristiansen LV, Romani S, Garcia-Alonso L, Hortsch M. 2004. Activation of EGF receptor kinase by L1-mediated homophilic cell interactions. Mol Biol Cell 15:2003–2012.

Itoh K, Cheng L, Kamei Y, Fushiki S, Kamiguchi H, Gutwein P, Stoeck A, Arnold B, Altevogt P, Lemmon V. 2004. Brain development in mice lacking L1–L1 homophilic adhesion. J Cell Biol 165:145–154.

Itoh K, Fushiki S, Kamiguchi H, Arnold B, Altevogt P, Lemmon V. 2005. Disrupted Schwann cell-axon interactions in peripheral nerves of mice with altered L1-integrin interactions. Mol Cell Neurosci 30:131–136.

Johnstone M, Goold RG, Fischer I, Gordon-Weeks PR. 1997. The neurofilament antibody RT97 recognises a developmentally regulated phosphorylation epitope on microtubule-associated protein 1B. J Anat 191:229–244.

Kamiguchi H, Lemmon V. 1998. A neuronal form of the cell adhesion molecule L1 contains a tyrosine-based signal required for sorting to the axonal growth cone. J Neurosci 18:3749–3756.

Kamiguchi H, Lemmon V. 2000a. IgCAMs: bidirectional signals underlying neurite growth. Curr Opin Cell Biol 12:598–605.

Kamiguchi H, Lemmon V. 2000b. Recycling of the cell adhesion molecule L1 in axonal growth cones. J Neurosci 20:3676–3686.

Kamiguchi H, Hlavin ML, Lemmon V. 1998a. Role of L1 in neural development: what the knockouts tell us. Mol Cell Neurosci 12:48–55.

Kamiguchi H, Long KE, Pendergast M, Schaefer AW, Rapoport I, Kirchhausen T, Lemmon V. 1998b. The neural cell adhesion molecule L1 interacts with the AP-2 adaptor and is endocytosed via the clathrin-mediated pathway. J Neurosci 18:5311–5321.

Kanemura Y, Takuma Y, Kamiguchi H, Yamasaki M. 2005. First case of L1CAM gene mutation identified in MASA syndrome in Asia. Congenit Anom (Kyoto) 45:67–69.

Kanemura Y, Okamoto N, Sakamoto H, Shofuda T, Kamiguchi H, Yamasaki M. 2006. Molecular mechanisms and neuroimaging criteria for severe L1 syndrome with X-linked hydrocephalus. J Neurosurg 105(5 Suppl):403–412.

Kenwrick S, Jouet M, Donnai D. 1996. X linked hydrocephalus and MASA syndrome. J Med Genet 33:59–65.

Kuhn TB, Stoeckli ET, Condrau MA, Rathjen FG, Sonderegger P. 1991. Neurite outgrowth on immobilized axonin-1 is mediated by a heterophilic interaction with L1(G4). J Cell Biol 115:1113–1126.

Kulahin N, Li S, Hinsby A, Kiselyov V, Berezin V, Bock E. 2008. Fibronectin type III (FN3) modules of the neuronal cell adhesion molecule L1 interact directly with the fibroblast growth factor (FGF) receptor. Mol Cell Neurosci 37:528–536.

Lagenaur C, Lemmon V. 1987. An L1-like molecule, the 8D9 antigen, is a potent substrate for neurite extension. Proc Natl Acad Sci U S A 84:7753–7757.

Law JW, Lee AY, Sun M, Nikonenko AG, Chung SK, Dityatev A, Schachner M, Morellini F. 2003. Decreased anxiety, altered place learning, and increased CA1 basal excitatory synaptic transmission in mice with conditional ablation of the neural cell adhesion molecule L1. J Neurosci 23:10419–10432.

Liljelund P, Ghosh P, van den Pol AN. 1994. Expression of the neural axon adhesion molecule L1 in the developing and adult rat brain. J Biol Chem 269:32886–32895.

Lindner J, Rathjen FG, Schachner M. 1983. L1 mono-and polyclonal antibodies modify cell migration in early postnatal mouse cerebellum. Nature 305:427–430.

Macias VR, Day DW, King TE, Wilson GN. 1992. Clasped-thumb mental retardation (MASA) syndrome: confirmation of linkage to Xq28. Am J Med Genet 43:408–414.

Maness PF, Schachner M. 2007. Neural recognition molecules of the immunoglobulin superfamily: signaling transducers of axon guidance and neuronal migration. Nat Neurosci 10:19–26.

Meech R, Kallunki P, Edelman GM, Jones FS. 1999. A binding site for homeodomain and Pax proteins is necessary for L1 cell adhesion molecule gene expression by Pax-6 and bone morphogenetic proteins. Proc Natl Acad Sci U S A 96:2420–2425.

Mintz CD, Dickson TC, Gripp ML, Salton SR, Benson DL. 2003. ERMs colocalize transiently with L1 during neocortical axon outgrowth. J Comp Neurol 464:438–448.

Mintz CD, Carcea I, McNickle DG, Dickson TC, Ge Y, Salton SR, Benson DL. 2008. ERM proteins regulate growth cone responses to Sema3A. J Comp Neurol 510:351–366.

Montgomery AM, Becker JC, Siu CH, Lemmon VP, Cheresh DA, Pancook JD, Zhao X, Reisfeld RA. 1996. Human neural cell adhesion molecule L1 and rat homologue NILE are ligands for integrin alpha v beta 3. J Cell Biol 132:475–485.

Munakata H, Nakamura Y, Matsumoto-Miyai K, Itoh K, Yamasaki H, Shiosaka S. 2003. Distribution and densitometry mapping of L1-CAM immunoreactivity in the adult mouse brain—light microscopic observation. BMC Neurosci 4:7.

Nakamura Y, Tamura H, Horinouchi K, Shiosaka S. 2006. Role of neuropsin in formation and maturation of Schaffer-collateral L1cam-immunoreactive synaptic boutons. J Cell Sci 119: 1341–1349.

Nishimura K, Yoshihara F, Tojima T, Ooashi N, Yoon W, Mikoshiba K, Bennett V, Kamiguchi H. 2003. L1-dependent neuritogenesis involves ankyrinB that mediates L1-CAM coupling with retrograde actin flow. J Cell Biol 163:1077–1088.

Ogawa Y, Schafer DP, Horresh I, Bar V, Hales K, Yang Y, Susuki K, Peles E, Stankewich MC, Rasband MN. 2006. Spectrins and ankyrinB constitute a specialized paranodal cytoskeleton. J Neurosci 26:5230–5239.

O'Gorman S, Dagenais NA, Qian M, Marchuk Y. 1997. Protamine-Cre recombinase transgenes efficiently recombine target sequences in the male germ line of mice, but not in embryonic stem cells. Proc Natl Acad Sci U S A 94:14602–14607.

Ohyama K, Tan-Takeuchi K, Kutsche M, Schachner M, Uyemura K, Kawamura K. 2004. Neural cell adhesion molecule L1 is required for fasciculation and routing of thalamocortical fibres and corticothalamic fibres. Neurosci Res 48:471–475.

Pavlou O, Theodorakis K, Falk J, Kutsche M, Schachner M, Faivre-Sarrailh C, Karagogeos D. 2002. Analysis of interactions of the adhesion molecule TAG-1 and its domains with other immunoglobulin superfamily members. Mol Cell Neurosci 20: 367–381.

Pratte M, Rougon G, Schachner M, Jamon M. 2003. Mice deficient for the close homologue of the neural adhesion cell L1 (CHL1) display alterations in emotional reactivity and motor coordination. Behav Brain Res 147:31–39.

Rathjen FG, Schachner M. 1984. Immunocytological and biochemical characterization of a new neuronal cell surface component (L1 antigen) which is involved in cell adhesion. EMBO J 3:1–10.

Rolf B, Kutsche M, Bartsch U. 2001. Severe hydrocephalus in L1-deficient mice. Brain Res 891:247–252.

Runker AE, Bartsch U, Nave KA, Schachner M. 2003. The C264Y missense mutation in the extracellular domain of L1 impairs protein trafficking in vitro and in vivo. J Neurosci 23:277–286.

Ruppert M, Aigner S, Hubbe M, Yagita H, Altevogt P. 1995. The L1 adhesion molecule is a cellular ligand for VLA-5. J Cell Biol 131:1881–1891.

Sakurai T, Lustig M, Babiarz J, Furley AJ, Tait S, Brophy PJ, Brown SA, Brown LY, Mason CA, Grumet M. 2001. Overlapping functions of the cell adhesion molecules Nr-CAM and L1 in cerebellar granule cell development. J Cell Biol 154:1259–1273.

Sakurai T, Gil OD, Whittard JD, Gazdoiu M, Joseph T, Wu J, Waksman A, Benson DL, Salton SR, Felsenfeld DP. 2008. Interactions between the L1 cell adhesion molecule and ezrin support traction-force generation and can be regulated by tyrosine phosphorylation. J Neurosci Res 86:2602–2614.

Sampo B, Kaech S, Kunz S, Banker G. 2003. Two distinct mechanisms target membrane proteins to the axonal surface. Neuron 37:611–624.

Schaefer AW, Kamei Y, Kamiguchi H, Wong EV, Rapoport I, Kirchhausen T, Beach CM, Landreth G, Lemmon SK, Lemmon V. 2002. L1 endocytosis is controlled by a phosphorylation-dephosphorylation cycle stimulated by outside-in signaling by L1. J Cell Biol 157:1223–1232.

Scotland P, Zhou D, Benveniste H, Bennett V. 1998. Nervous system defects of AnkyrinB (-/-) mice suggest functional overlap between the cell adhesion molecule L1 and 440-kD AnkyrinB in premyelinated axons. J Cell Biol 143:1305–1315.

Shin DH, Lee KS, Lee E, Cho SS, Kim J, Kim JW, Kwon BS, Lee HW, Lee WJ. 2003. The correspondence between the labeling patterns of antibody RT97, neurofilaments, microtubule associated protein 1B and tau varies with cell types and development stages of chicken retina. Neurosci Lett 342:167–170.

Stallcup WB, Beasley L. 1985. Involvement of the nerve growth factor-inducible large external glycoprotein (NILE) in neurite fasciculation in primary cultures of rat brain. Proc Natl Acad Sci U S A 82:1276–1280.

Triana-Baltzer GB, Liu Z, Berg DK. 2006. Pre-and postsynaptic actions of L1-CAM in nicotinic pathways. Mol Cell Neurosci 33:214–226.

Triana-Baltzer GB, Liu Z, Gounko NV, Berg DK. 2008. Multiple cell adhesion molecules shaping a complex nicotinic synapse on neurons. Mol Cell Neurosci 39:74–82.

Tybulewicz VL, Crawford CE, Jackson PK, Bronson RT, Mulligan RC. 1991. Neonatal lethality and lymphopenia in mice with a homozygous disruption of the c-abl proto-oncogene. Cell 65: 1153–1163.

Venero C, Tilling T, Hermans-Borgmeyer I, Herrero AI, Schachner M, Sandi C. 2004. Water maze learning and forebrain mRNA expression of the neural cell adhesion molecule L1. J Neurosci Res 75:172–181.

Voas MG, Lyons DA, Naylor SG, Arana N, Rasband MN, Talbot WS. 2007. AlphaII-spectrin is essential for assembly of the nodes of Ranvier in myelinated axons. Curr Biol 17:562–568.

Weller S, Gartner J. 2001. Genetic and clinical aspects of X-linked hydrocephalus (L1 disease): mutations in the L1CAM gene. Hum Mutat 18:1–12.

Whittard JD, Sakurai T, Cassella MR, Gazdoiu M, Felsenfeld DP. 2006. MAP kinase pathway-dependent phosphorylation of the L1-CAM ankyrin binding site regulates neuronal growth. Mol Biol Cell 17:2696–2706.

Wiencken-Barger AE, Mavity-Hudson J, Bartsch U, Schachner M, Casagrande VA. 2004. The role of L1 in axon pathfinding and fasciculation. Cereb Cortex 14:121–131.

Wisco D, Anderson ED, Chang MC, Norden C, Boiko T, Folsch H, Winckler B. 2003. Uncovering multiple axonal targeting pathways in hippocampal neurons. J Cell Biol 162:1317–1328.

Wolfer DP, Mohajeri HM, Lipp HP, Schachner M. 1998. Increased flexibility and selectivity in spatial learning of transgenic mice ectopically expressing the neural cell adhesion molecule L1 in astrocytes. Eur J Neurosci 10:708–717.

Yamasaki M, Thompson P, Lemmon V. 1997. CRASH syndrome: mutations in L1CAM correlate with severity of the disease. Neuropediatrics 28:175–178.

Yap CC, Nokes RL, Wisco D, Anderson E, Folsch H, Winckler B. 2008. Pathway selection to the axon depends on multiple targeting signals in NgCAM. J Cell Sci 121:1514–1525.